

Palacký University Olomouc

Faculty of Science

Department of Geology



**Effect of Fe₂O₃/Xanthan nanocomposites on wettability
alteration under different reservoir conditions**

Bachelor thesis

Aban Shorrsh Bilal

Petroleum Engineering (B0724A330002)

Fulltime study

Supervisor: RNDr. Jagar Ali , Ph. D.

Olomouc 2023

Effect of Fe₂O₃/Xanthan nanocomposites on wettability alteration under different reservoir conditions

Anotace:

Produkce může být náročná na ropných polích uhličitane ropy. Vylepšené systémy rekuperace ropy snižují mezifázové napětí (IFT) a zvyšují účinnost přemístění. V aplikacích EOR se nanokompozity stále více používají pro své klíčové vlastnosti, protože mají velký vliv na mezifázové napětí a změnu smáčivosti. Tato práce se zaměřila na pochopení toho, jak může nanokompozit Fe₂O₃/xanthan (NC) ovlivnit mezifázové napětí a změnu smáčivosti při různých třech odlišných koncentracích NC (250 ppm, 500 ppm a 1000 ppm), třech různých teplotách (30 °C, 50 °C a 70 °C) a tři různé tlaky (500 psi, 1000 psi a 1500 psi), kontaktní úhel a IFT byly určeny v DW a SW. co toto šetření objevilo jako Nejlepší IFT byl v DW a bylo zjištěno, že je 1,141 mN/mv 500 ppm při 30 °C a tlaku 1000. Nejlepší kontaktní úhel byl nalezen v DW, který byl zjištěn při 250 ppm při 30 °C při 500 psi, což snížilo kontaktní úhel na 47,34 stupně.

Effect of Fe₂O₃/Xanthan nanocomposites on wettability alteration under different reservoir conditions

Annotation:

Production can be challenging in oil-wet carbonate oil fields, Improved oil recovery systems reduce interfacial tension (IFT) and boost displacement efficiency. In EOR applications, nanocomposites are increasingly being used for its crucial proprieties for having a great affect on interfacial tension and wettability alteration. This work focused on understanding how Fe₂O₃/xanthan nanocomposite (NC) can effect on interfacial tension and wettability alteration under different three distinct NC concentrations of (250 ppm, 500 ppm, and 1000 ppm), three different temperatures (30 C°, 50 C°, and 70 C°), and three different pressures (500 psi, 1000 psi, and 1500 psi), the contact angle and IFT were determined in DW and SW. what this investigation discovered as The best IFT was in DW and it was found to be 1.141 mN/m in 500ppm at 30 °C and 1000 pressure. The best contact angle was found in DW which was found to be in 250 ppm at 30 C° at 500 psi that reduced the contact angle to 47.34 degree.

Keywords: interfacial tension, Contact angle, Distilled water, Salinity water, Pressure, Temperature.

Number of pages: 56

Number of annexes: None

I declare that I have prepared the bachelor's thesis myself and that I have stated all the used information resources in the thesis.



Shorrsh Bilal

Aban

In Olomouc, May 27, 2022

Acknowledgement

I would like to express my special thanks to my mentor Dr.Jagar Ali for his time and efforts he provided throughout the year. Your useful advice and suggestions were really helpful to me during the bachelor thesis completion. In this aspect, I am eternally grateful to you. I would like to express my gratitude to all individuals involved with the laboratory of the Department of Petroleum Engineering at Soran University. Their crucial help and expertise in operating technical laboratory equipment and following to safety protocols during the testing phase of this study are greatly appreciated. Finally, I would like to express my sincere gratitude and appreciation to my family, relatives, and friends during my academic journey. I would like to express my deepest appreciation to my parents for their vital inspiration, unwavering encouragement, and constant motivation. Thank you greatly.

Table of contents

CHAPTER 1: INTRODUCTION AND OBJECTIVES	1
1.1 Introduction.....	1
1.2 Objectives.....	1
1.3 Outlines.....	2
CHAPTER 2: BACKGROUND AND LITERATURE REVIEW	3
2.1. Petroleum reservoir.....	3
2.2. reservoir rock properties	4
2.2.1 Porosity	4
2.2.2 Permeability	6
2.2.3 Saturation	7
2.2.4 Capillary pressure	7
2.2.5. Wettability	8
2.3. Recovery mechanism.....	9
2.4. Chemical EOR	10
2.5. Nano-EOR	11
2.6. EOR in different reservoir conditions.....	19
CHAPTER 3: MATERIALS AND METHODOLOGYERROR! BOOKMARK NOT	DEFINED.
3.1 Materials	22
3.2 Methodology.....	23
3.2.1 Preparation of nanofluid	23
3.2.2 Preparation of rock thin sections	24
3.3.3 Interfacial tension measurement	25
3.3.4. contact angle measurement.....	25
CHAPTER 4: RESULTS AND DISCUSSION	27
4.1 Characterization of nanocomposites.....	27

4.2 Effect of NCs on wettability alteration	28
4.3 Effect of NCs on interfacial tension	34
CHAPTER 5: CONCLUSIONS AND RECOMMENDATIONS	38
5.1 conclusion	38
5.2 recommendation.....	38
REFERENCES	39

List of Figures

FIGURE 1 ILLUSTRATION OF A TYPICAL OIL AND GAS RESERVOIR (FERNANDES ET AL., 2014).	4
FIGURE 2 SIMPLIFIED EXAMPLES OF MATERIALS WITH HIGH AND LOW POROSITY (KLITGAARD, 2022).....	5
FIGURE 3 LOW PERMEABILITY AND HIGH PERMEABILITY DIFFERENCES (GANAT, 2019).....	6
FIGURE 4 CONTACT ANGLE (ABDALLAH ET AL. 2007)	9
FIGURE 5 OIL RECOVERY METHODS AND TECHNIQUES FROM THE PRIMARY TO THE TERTIARY PHASE MODIFIED AFTER (ADENIYI, Nwalor and AKO, 2008).....	10
FIGURE 6 FLOW SHEET FOR EOR METHODS (ELSHARAFI, 2019).....	11
FIGURE 7 MECHANISMS OF NANOFLUID WITHIN THE POROUS MEDIA (ALI ET AL., 2018).	12
FIGURE 8 PLOTTED GRAPH OF EXPERIMENTAL DATA OF REDUCTION PERCENTAGE OF THE INTERFACIAL TENSION USING DIFFERENT NPs.....	14
FIGURE 9 FLUID DISTRIBUTIONS IN (A) WATER-WET AND (B) OIL-WET ROCK (ALI ET AL., 2018).	15
FIGURE 10 PLOTTED GRAPH OF OBTAINED EXPERIMENTAL DATA OF DIFFERENT NANOPARTICLES.....	18
FIGURE 11 ZETA POTENTIAL VALUES OF NPs IN HSM (NO SALT ADDED), AND UNDER TWO SALINITY CONDITIONS (10 AND 32 G L ⁻¹).....	20
FIGURE 12 HYDRODYNAMIC DIAMETER DISTRIBUTION OF Fe ₃ O ₄ AND CuO PARTICLE SIZE IN HSM (DOTS), AND UNDER TWO SALINITY CONDITIONS, 10 G L ⁻¹ (DASH) AND 32 G L ⁻¹ (LINE) (CANUEL ET AL., 2021).	21
FIGURE 13 EFFECTIVE THERMAL CONDUCTIVITIES OF NANOFLUIDS AGAINST STANDING TIME AT DIFFERENT TEMPERATURES.	21
FIGURE 14 THE ROCK SAMPLE AND NANO-COMPOSITE THAT USED IN THIS STUDY.....	23
FIGURE 15 THE DEVICES ARE USED TO PREPARE NCs AND MEASURE THEIR CHARACTERISTICS.	24
FIGURE 16 THE PROCEDURE OF PREPARING ROCK THIN SECTIONS IN THIS STUDY	25
FIGURE 17 THE IFT AND CONTACT ANGLE MEASUREMENTS USED IN THIS STUDY	ERROR!
BOOKMARK NOT DEFINED.	
FIGURE 18 AGEING PROCEDURE OF THIN SECTION	26
FIGURE 19 IMPACT OF NF CONCENTRATION ON A) CONDUCTIVITY B) VISCOSITY C)PH AND D) DENSITY	26

FIGURE 20 IFT VALUES IN DW AND SW IN THREE DIFFERENT CONCENTRATIONS (250PPM,500PPM,1000PPM) AND PRESSURES WITH CONSTANT TEMPERATURE A) 30C, 500 PSI. B) 30C, 1000PSI. C) 30C, 1500 PSI. 35

FIGURE 21 IFT VALUES IN DW AND SW IN THREE DIFFERENT CONCENTRATIONS (250PPM,500PPM,1000PPM) AND PRESSURES WITH CONSTANT TEMPERATURE A) 50C, 500 PSI. B) 50C, 1000PSI. C) 50C, 1500 PSI. 35

FIGURE 22 IFT VALUES IN DW AND SW IN THREE DIFFERENT CONCENTRATIONS (250PPM,500PPM,1000PPM) AND PRESSURES WITH CONSTANT TEMPERATURE A) 70C, 500 PSI. B) 70C, 1000PSI. C) 70C, 1500 PSI. 36

List of Tables

TABLE 1 METHODS, MECHANISMS AND CHALLENGES OF CHEMICAL EOR.....	11
TABLE 2 A SUMMARY OF PREVIOUS WORKS ON EFFECTS OF NANOPARTICLES ON INTERFACIAL TENSION (IFT).....	14
TABLE 3 A SUMMARY OF PREVIOUS WORKS ON EFFECTS OF NANOPARTICLES ON CONTACT ANGLE.	16
TABLE 4 COMPOSITION OF CRUDE OIL AND BRINE.....	22
TABLE 5 EFFECT OF TEMPERATURE AND NANO CONCENTRATION OF CONTACT ANGLE IN 500 PSI.	29
TABLE 6 EFFECT OF TEMPERATURE AND NANO CONCENTRATION OF CONTACT ANGLE IN 1000 PSI.	31
TABLE 7 EFFECT OF TEMPERATURE AND CONCENTRATION ON CONTACT ANGLE IN 1500 PSI.	33

List of abbreviations

CA	Contact angle
CEOR	Chemical enhanced oil recovery
COBR	Crude oil brine rock
DW	Distilled water
EOR	Enhanced oil recovery
EDTA	Ethylene diamine tetra-acetic acid
HSM	High salt medium
IFT	Interfacial tension
LR	Literature review
Pc	Capillary pressure
SW	Salt water

Chapter 1: Introduction and objectives

1.1 Introduction

A significant amount of present global oil production originates from aging fields, and the pace of replacement of produced reserves by new discoveries has been continuously dropping over the previous few decades. In the years to come, recoverable oil resources in identified reservoirs that can be produced inexpensively utilizing enhanced IOR and EOR technologies will assist meet global energy demand. (Manrique, 2010). Residual oil is known to stay after waterflooding and EOR will help to produce residual oil Sheng (2015). Basic oil recovery methods have the potential to recover 18-20% of OOIP. EOR recovers additional crude oil from reservoirs with a 30-60% recovery factor. Nanomaterials have a larger surface area than large-scale materials of an identical mass and They're dense. More material can touch the external environment when the surface area per mass increases (Sircar et al., 2021). The peculiar physicochemical features of nanoparticles have piqued the interest of several industries, including petroleum. Nanoscience is used or explored in remote locations such as arctic and severe deep sea environments, as well as unconventional reservoirs, in every major sector of these industries, including exploration, drilling, monitoring, producing, processing, and distribution. Production is notable (Shingala et al., 2020). The purpose of this work is to investigate the impact of nanoparticles on wettability and interfacial tension under various reservoir conditions.

1.2 Objectives

The goal of this study is to investigate the effect of various nanocomposite additive concentrations on the interfacial tension and wettability alteration at various temperatures and pressures. As a result, three distinct concentrations ($\text{Fe}_2\text{O}_3/\text{xanthan}$) nanocomposite of in smart water, and distilled water are employed as chemical substances in EOR operations. Then, investigate the impacts of quantifiable ($\text{Fe}_2\text{O}_3/\text{xanthan}$) nanocomposite in the EOR process.

Moreover, the following are the study objectives:

- 1- Effect of ($\text{Fe}_2\text{O}_3/\text{xanthan}$) nanocomposite on IFT
- 2- Effect of ($\text{Fe}_2\text{O}_3/\text{xanthan}$) nanocomposite on wettability alteration

1.3 Outlines

The report is divided into five sections. The initial section comprises an introductory segment, objectives, and an overview of the report's structure. Section two comprises of background information and a literature review encompassing various aspects such as reservoir rock properties, including porosity, permeability, and saturation. Additionally, it covers capillary pressure, oil recovery mechanisms, chemical enhanced oil recovery mechanisms techniques, the impact of nanotechnology in EOR, the influence of salinity on nanofluid performance, as well as the effects of pressure and temperature on nanofluid performance. Section three of this report provides an in-depth analysis of the materials and processes employed in the course of this investigation. Section 4 contains results and conclusions. The final part includes a summary of the results and further recommendations.

Chapter 2: Background and literature review

2.1. Petroleum reservoir

Petroleum reserves may contain either natural gas, oil, or a combination of both. Some of the essential features of the subject include the thickness of the pay zone, the lithology of the rock, the porosity of the rock, the total compressibility, and the permeability of the rock. These particular attributes have a significant influence on the flow of reservoir fluids, subsequently impacting the efficiency of the well. In order to accurately simulate reservoir behavior and predicted well productivity, it is imperative for reservoir engineers to possess a comprehensive understanding of the qualities outlined by (Guo et al. 2008). Sedimentary rocks commonly harbor petroleum reserves. Petroleum is rarely found in igneous or metamorphic rocks that exhibit fractures. Igneous and metamorphic rocks are typically formed in high-pressure, high-temperature environments, which are generally unfavorable for the formation of petroleum reserves. Frequently, these formations exhibit insufficient permeability or interconnected pore space, which hinders the establishment of a pathway for petroleum to migrate towards a wellbore. The metamorphic rock has experienced significant pressure and heat, despite its initial composition as sandstone. Any petroleum fluid that may have previously occupied the pores has been evaporated. According to Fanchi (2010), sedimentary rock is the type of rock that is most probable to contain significant amounts of petroleum. Reservoirs refer to permeable porous mediums that constitute oil-bearing rock formations. The trap, seal, or cap rocks are impermeable formations that are commonly employed to surround these reservoirs. In reservoir conditions, the hydrocarbons contained within the rock pores can display complex phase behavior, potentially transitioning into various phases including oil, gas, alternative liquids, or solid forms such as asphaltene. In oil reservoirs, the presence of water is a constant, resulting in the existence of an aqueous phase at all times. The process of drilling wells to establish a connection between the reservoir and the surface is necessary in order to extract oil from the fields. Figure 1 displays a well that has been drilled into the formation. The implementation of secondary recovery, also referred to as reservoir pressure maintenance, involves the injection of water or recycled gas into the reservoir. This practice effectively increases the reservoir pressure and enables sustained production. Tertiary recovery, also

referred to as improved oil recovery (IOR), pertains to any method of oil recovery that falls outside the primary or secondary recovery categories (enhanced oil recovery, or EOR). The Enhanced Oil Recovery (EOR) encompasses various techniques, including but not limited to heat recovery, gas flooding, and chemical injection. Enhanced oil recovery (EOR) procedures have the potential to recover up to 60% of the original oil in place, surpassing the recovery rates of primary and secondary methods, which stand at 20% and 40% accordingly. It is important to acknowledge that the type of oil and the depth of the reservoir have an influence on the recoverable quantities, as stated by Fernandes et al. (2014).

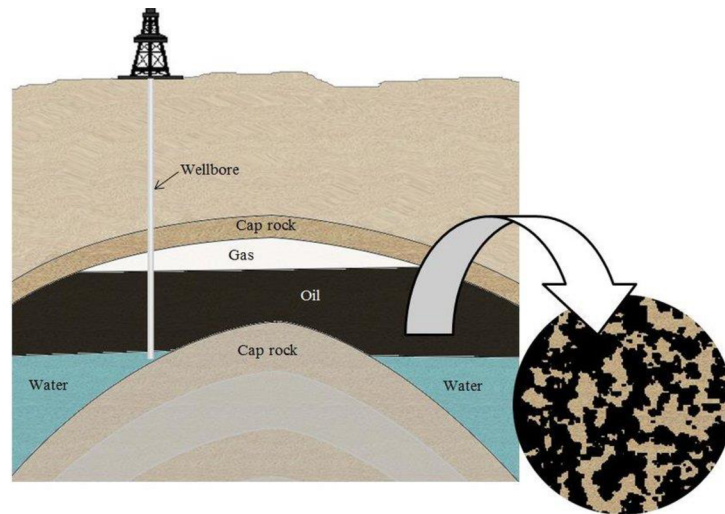


Figure 1 Illustration of a typical oil and gas reservoir (Fernandes et al., 2014).

2.2. reservoir rock properties

2.2.1 Porosity

The pore fraction of reservoir rock—that is, the ratio of pore space volume to bulk volume of the rock—is characterized as its porosity. The proportion of porosity is commonly used:

$$\Phi = \frac{V_{pore}}{V_{bulk}} \quad (\text{Eq.1})$$

Porosities in fluid-productive sandstones range between 0.05 and 0.4, or 5%-40%. (Guo et al. 2008). The term porosity refers to the ratio of pore volume to total bulk volume of a rock. A rock with a high porosity may hold more oil per volume unit. Figure 2 depicts a simplified version of this. Increased burial depth often results in compaction of the sediments, resulting in lower porosity (Gill and Simon, 1998). Every form of rock may serve as a reservoir as long as the pore space is large enough to hold fluids and well linked enough to facilitate

flows. Nonetheless, sedimentary rocks such as sandstones and carbonates are the most common reservoir types, and sedimentary reservoirs account for the majority of the world's known oil fields. More than 15% porosity is deemed good or even excellent for oil reservoirs deemed good or even excellent for oil reservoirs considered good or perhaps excellent (Klitgaard, 2022).

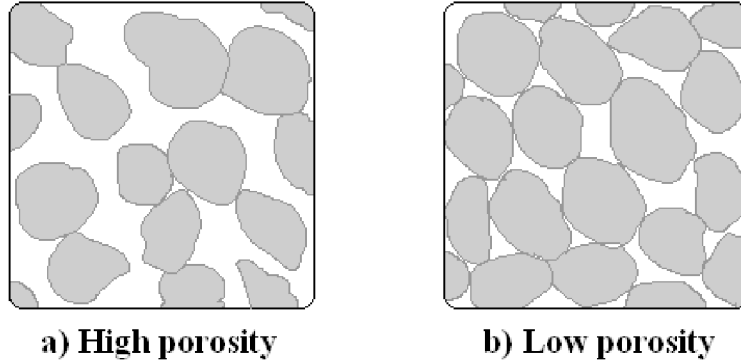


Figure 2 Simplified examples of materials with high and low porosity (Klitgaard, 2022).

2.2.2 Permeability

The flow of the hydrocarbon will be permitted only if the reservoir rocks have appropriate permeability, which is an important criterion in reservoir engineering. Fluid permeability is defined as the ability of fluids to flow through porous media. It measures the ability of fluid to move from the porous medium through the reservoir rock to the producing well's wellbore; the higher the permeability, the faster the fluid flows. Permeability is an important metric because it affects the pace at which oil and gas may be recovered. The reservoir engineer strives to establish this as the most critical parameter. Permeability typically ranges from less than 0.01 millidarcy (mD) to greater than 1 Darcy. While permeability values of 0.1 mD are often regarded low for oil reservoirs, they are nevertheless practical for gas reservoirs. The permeability of highly productive reservoirs is often tested in the Darcy range. Normally, a reservoir with low porosity would be impermeable to a fluid, whereas a reservoir with large porosity would also be impermeable (i.e. zero permeability), as illustrated in Fig 3 When drilled, such a reservoir rock will not generate hydrocarbons (Ganat, 2019).

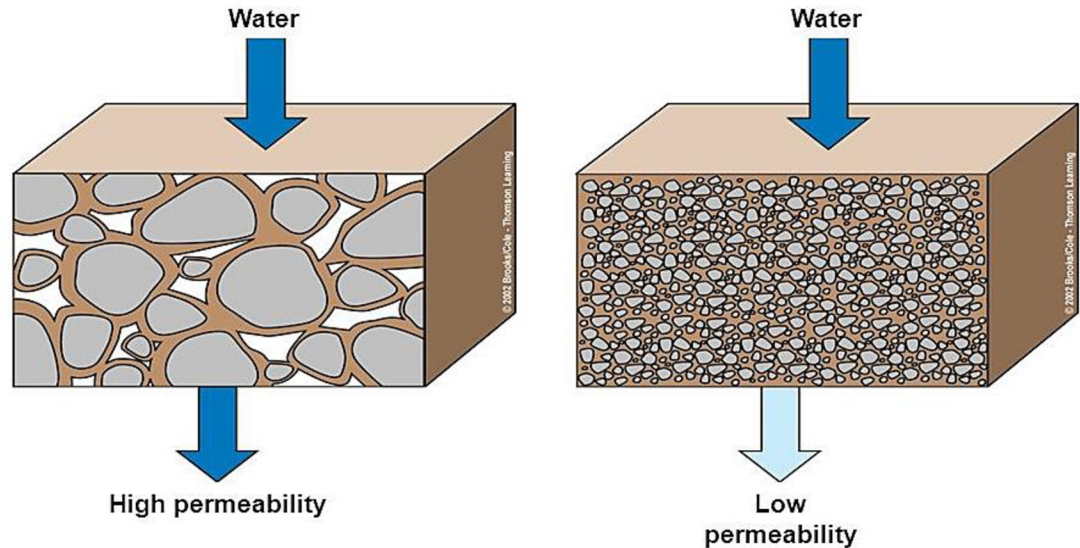


Figure 3 low permeability and high permeability differences (Ganat, 2019)

2.2.3 Saturation

The carbonate reservoir commonly found in the Middle East exhibits significant potential. However, the challenges arise from its low permeability and high gas-oil ratio, which obscure the understanding of reservoir saturation and pressure distribution. Consequently, the development of such reservoirs becomes exceedingly complex. The assessment of reservoir performance in the future heavily relies on the critical indicators of oil saturation and the distribution of remaining oil (Wei et al., 2022). Prior to the process of migration and trapping, the majority of oil deposits were found to be saturated with water. Lighter hydrocarbons displace water, restoring it to a state of hydrostatic and dynamic equilibrium. According to Zhang (2019), water cannot be fully substituted by oil within pores. The pore volume of a fluid can be defined as the percentage of saturation.

Each phase's saturation has a range of possibilities ranging from 0% to 100%. The oil must surpass a specific threshold in order to facilitate its flow. In all instances, saturations are estimated using pore volume rather than the gross volume of the reservoir. This suggests that the oil is confined within the pores and does not exhibit fluid-like behavior. As stated by Zhang (2019), an additional measure of importance known as mobile oil saturation (Som) can be defined as the proportion of pore volume occupied by mobile oil, as represented by the following equation:

2.2.4 Capillary pressure

The use of capillary pressure concepts allows for the evaluation of numerous variables related to reservoir rock quality, expected reservoir fluid saturations, depths of fluid contacts, transition zone thickness, seal capacity, pay versus non pay resolve, and recovery efficiency calculation. These aspects are as follows: (Vavra et al., 1992). The capillary pressure within a reservoir plays a crucial role in determining the distribution of saturation, which in turn affects the overall volumes of fluids present in the reservoir, including oil, water, and gas. Having precise understanding of the distribution of capillary pressure during drainage is a crucial factor in ensuring the dependable estimation of hydrocarbon reserves. The concept

of imbibition capillary pressure is used to characterize the displacement processes of reservoir fluids during production operations, as well as to analyze and interpret the outcomes of relative permeability experiments (McPhee et al., 2015). In high-permeability rocks with correspondingly large pore radius, capillary pressure (P_c) is lower. Capillary pressure cannot be directly measured in a reservoir. Capillary pressure, on the other hand, is usually measured by centrifuge studies on water reservoirs. Capillary pressure measurements are used in reservoir engineering to determine two important reservoir phenomena, which are listed below. Because it governs the flow of fluids between the crack and the rock matrix, capillary pressure is particularly important in explaining fluid flow from fractured reservoirs. Since it influences the flow of fluids between the crack and the rock matrix, it is useful in understanding fluid flow from fractured reservoirs. As a result, capillary pressure is proportional to IFT, contact angle, and pore radius in the following way. Figure 4 depicts a capillary pressure curve, and the height (h) of a transition zone above a free water level.

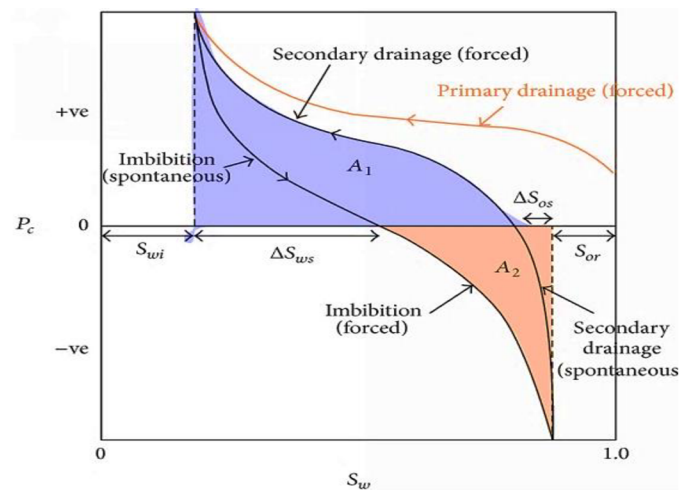


Figure 4 Capillary pressure diagram (McPhee, et al. 2015).

2.2.5. Wettability

To improve oil recovery, it is essential to have a solid understanding of the wettability of the deposit. The tendency for oil soaking rather than water wetting has an influence on several aspects of reservoir performance, most notably water flooding and enhanced oil recovery procedures. If it is assumed that a reservoir has moisture when in fact it does not, the reservoir may sustain damage that cannot be repaired. The degree to which a solid prefers to interact with one fluid over another is referred to as its wettability. When one fluid is

selectively wetter than another, a drop of the selectively wetter will displace the other fluid and, at its most extreme, will spread across the whole surface. On the other hand, if you drop a nonwetting fluid onto a surface that is covered with a wetting fluid, the fluid will bead up, reducing the amount of contact it has with the solid. If the condition is neither substantially water wetting nor strongly oil wetting, then the equilibrium of forces in the oil/water/solid system will generate a contact angle between the fluids at the solid surface. (Abdallah et al. 2007)

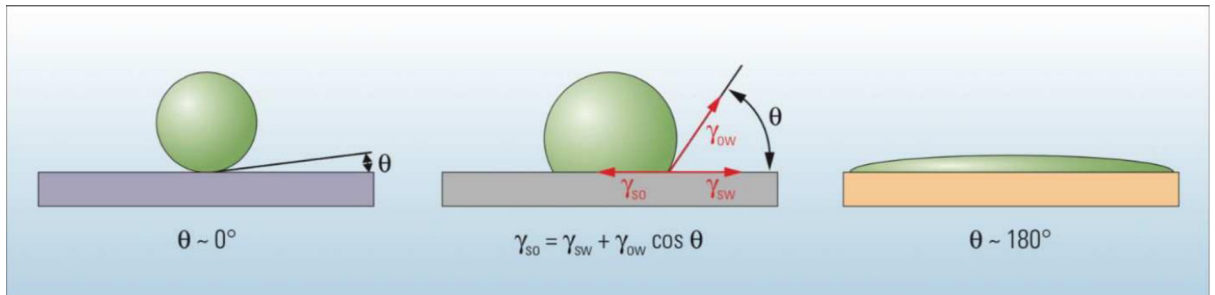


Figure 4 Contact angle (Abdallah et al. 2007)

Adhesion is a phenomenon that happens when the particles of a liquid and a solid come into touch with one another. Calculating adhesion entails estimating the force or amount of work necessary to separate phases such as liquid and solid per unit area. The contact angle formed by the forces of adhesion among a liquid and a solid surface when the liquid comes into contact with the solid surface. When the adhesive strength of a liquid to a solid is greater than the liquid's cohesion forces (the liquid wets the surface of the solid), the angle is extremely small (90 degrees).

2.3. Recovery mechanism

Primary, secondary, and tertiary oil recovery are the traditional designations for hydrocarbon recovery in sequence of creation. Primary oil recovery extracts hydrocarbons without the addition of gas or water by using the reservoir's inherent driving forces. Because most reservoirs lack enough natural drive, artificial drive injection has become routine practice. The most basic method is to inject gas or water. Water and immiscible gas injection have the potential to extract additional oil. The selected secondary recovery technique is

normally performed after the primary recovery, although it might be performed simultaneously. Water inundation is used in the majority of secondary recovery strategies. It must, however, be shown that natural healing processes are insufficient to enable continued recovery. Otherwise, the significant financial investment in a secondary recovery effort may be squandered. (Ahmed, 2010).

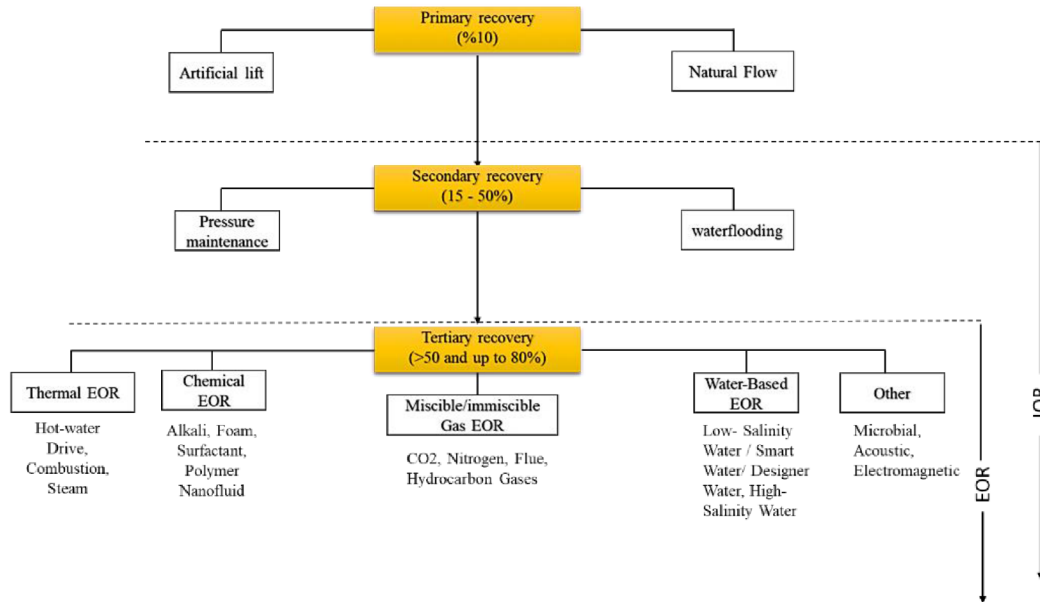


Figure 5 Oil recovery methods and techniques from the primary to the tertiary phase modified after (Adeniyi, et al. 2008).

2.4. Chemical EOR

Given the escalating global energy demand and the depletion of energy resources, it is imperative to prioritize the optimization of oil recovery from previously untapped reserves. This is essential in order to effectively address the continuously growing energy demand (Barman et al., 2001). Oil and gas continue to be the dominant sources of energy production across the world, notwithstanding the progress that has been achieved in renewable energy. In the meanwhile, despite the adoption of conventional oil recovery strategies, significant quantities of oil reserves remain unrecovered. It has been determined that chemical enhanced oil recovery, often known as EOR, is an effective method for recovering oil that has been bypassed as well as residual oil that has been trapped in the reservoir. In order to maximize oil recovery, this EOR strategy involves the injection of several chemicals (Gbadamosi et al., 2019). By definition, enhanced oil recovery is the recovery of oil by the injection of

chemicals, gases, and/or thermal energy into the reservoir. Tertiary oil recovery, commonly known as enhanced oil recovery (EOR), is the third stage of extraction of oil from a reservoir. Figure 6 depicts a more expensive and common procedure. Tertiary recovery is generally accomplished by gas or chemical injections, as well as heat recovery (Maroufi et al., 2013).

Table 1 Methods, mechanisms and challenges of chemical EOR.

Chemical EOR types	Challenges	Mechanism
Polymer flooding	Wettability alteration	Fingering
Surfactant flooding	Reduced IFT	High cost
Alkaline flooding	Control mobility	Sensitivity to salinity and heat
ASP flooding		
Nano particles		

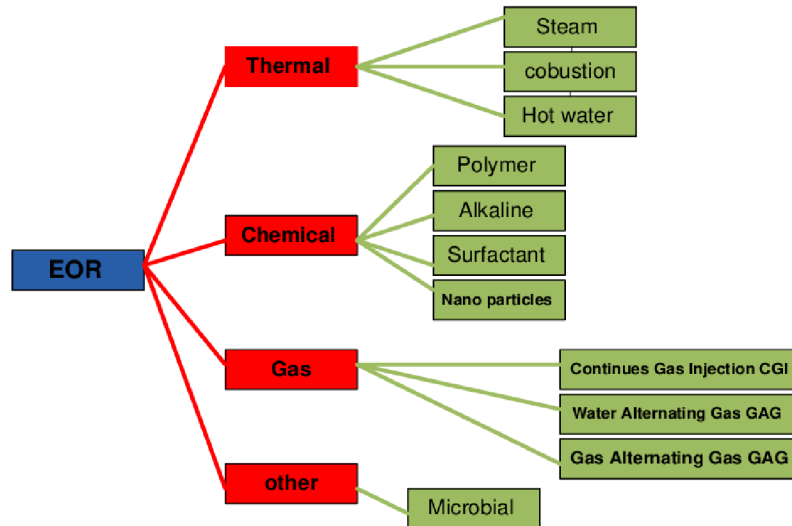


Figure 6 Flow sheet for EOR methods (Elsharafi, 2019).

2.5. Nano-EOR

As shown in Figure 7, an interfacial tension force (IFT) is produced when immiscible fluids like crude oil and water coexist in oil reservoirs. . IFT is the energy per unit area that forces the molecule toward the surface from the bulk phase. It is typically measured in dynes/cm (milli-Newtons/meter), which is a SI unit of measurement. In order to analyze fluid distribution and movement in porous medium, it is possible to make use of IFT, which is one of the main properties. As a direct consequence of this, IFT has a significant bearing on the reservoir's capacity to produce hydrocarbons. According to Ahmadi and Shadizadeh (2017), assessing the interfacial tension between oil and brine or oil and injected fluids is essential to assessing improved oil recovery strategies. The interfacial tension (IFT) between the brine and oil phases may be measured using a spinning drop tensiometer. In the event that a micro-emulsion is found to be a third phase in any given situation, the oil phase may be considered a middle phase in order to provide more accurate IFT measurements in the study carried out by Zhang et al. (2012). According to Ahmadi et al. (2017), in order to avoid residual oil saturation, it is essential to have a high capillary number as well as a low interfacial tension (IFT) between water and oil.

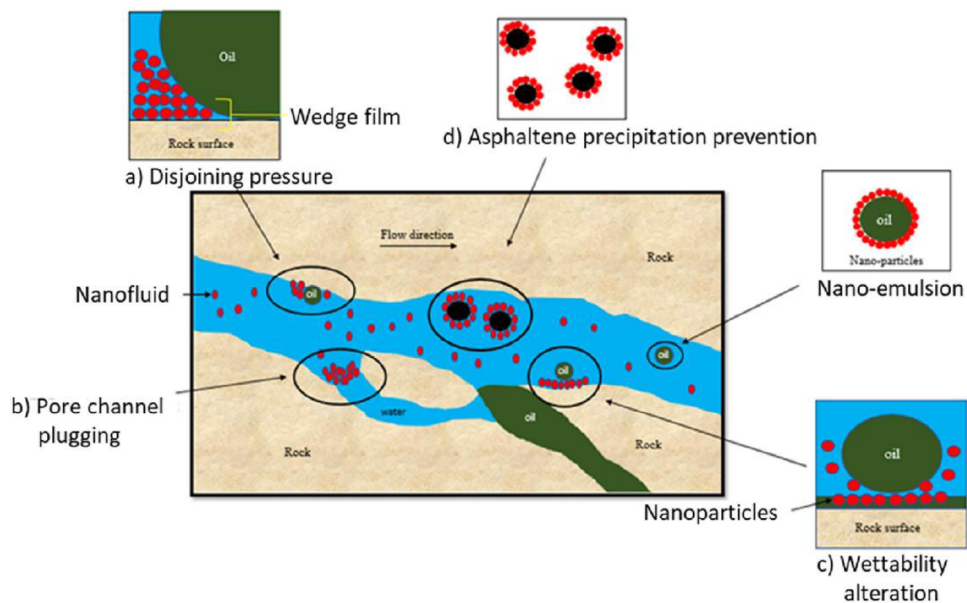


Figure 7 Mechanisms of nanofluid within the porous media (Ali et al., 2018).

Table 2 stating the summarized data of conducted experiment by the following researchers: (Li, Hendraningrat and Torsaeter, 2013), (El Shafey, 2017), (Zargartalebi, Barati and Kharrat, 2014), (Emadi et al., 2017), (Hendraningrat and Torsæter, 2014), (Azarshin, Moghadasi and A Aboosadi, 2017),(Mahbubul, 2019), (Esfandyari Bayat et al., 2014),(Roustaei et al., 2012), (Joonaki and Ghanaatian, 2014),(Roustaei, Saffarzadeh and

Ccategory	NPs	NPs size (nm)	NPs Conc.	Dispersion media	IFT reduction (%)		CA	Oil recovery	Ref.
					Clean	With NPs			
nanomaterials	FNP	7–16	0.05 wt%	DIW	16.41	12.61	124	23,1 %	(Hendraningrat, Li and Torsaeter, 2013)
	CNP	8–75	0.05 wt%	DIW	16.41	12.15	40	25.9%	
	SiO ₂	20–30	5 wt%	Surfactant	35	10.9	38.82	68.8%	(Emadi et al., 2017)
	SiO ₂	40	0.05 wt%	Brine	19.2	17.5	28.6	8.85%	(Hendraningrat and Torsæter, 2014)
	Al ₂ O ₃	17	0.05 wt%	Brine	19.2	12.8	59.7	33.3%	(Hendraningrat and Torsæter, 2014)
	SiO ₂	10–15	10 gr/200 ml	Ethanol	37.5	22.1	98.2	43.7%	(Azarshin, Moghadasi and A Aboosadi, 2017)
nanocomposites	FSPNs	10–15	10 g/200 ml	Ethanol	37.5	13	68.5	65.3%	(Azarshin, Moghadasi and A Aboosadi, 2017)
	Al ₂ O ₃	20	0.05 wt%	CTAB	8.46	1.65	103.5	80.5%	(Mahbubul, 2019)
	Al ₂ O ₃	20	0.05 wt%	SDS	9.88	2.75	66	80.3%	(Mahbubul, 2019)
	Al ₂ O ₃	20	0.05 wt%	TX-100	9.13	2.55	54.52	72.1%	(Mahbubul, 2019)
	ZrO ₂	40	0.05 wt%	CTAB	8.46	1.85	23.71	42.6%	(Mahbubul, 2019)
	ZrO ₂	40	0.05 wt%	SDS	9.88	2.78	~0	71.8%	(Mahbubul, 2019)
	ZrO ₂	40	0.05 wt%	TX-100	9.13	2.64	52	71.1%	(Mahbubul, 2019)
	Al ₂ O ₃	40	50 mg/L	DIW (26 °C)	26.5	18	75	32%	(Esfandyari Bayat et al., 2014)
	TiO ₂	10–30	50 mg/L	DIW (26 °C)	26.5	17.5	62	33.9%	(Esfandyari Bayat et al., 2014)
	SiO ₂	20	50 mg/L	DIW (26 °C)	26.5	17	60	35.8%	(Esfandyari Bayat et al., 2014)
	Al ₂ O ₃	40	50 mg/L	DIW (60 °C)	21.1	13.2	84	37.5%	(Esfandyari Bayat et al., 2014)
	TiO ₂	10–30	50 mg/L	DIW (60 °C)	21.1	12.4	71	41.2%	(Esfandyari Bayat et al., 2014)
SiO ₂	20	50 mg/L	DIW (60 °C)	21.1	11.2	46	46.9%	(Esfandyari Bayat et al., 2014)	

Mohammadi, 2013), (Esmaeilzadeh et al., 2014)

Table 2 A summary of previous works on effects of nanoparticles on interfacial tension (IFT).

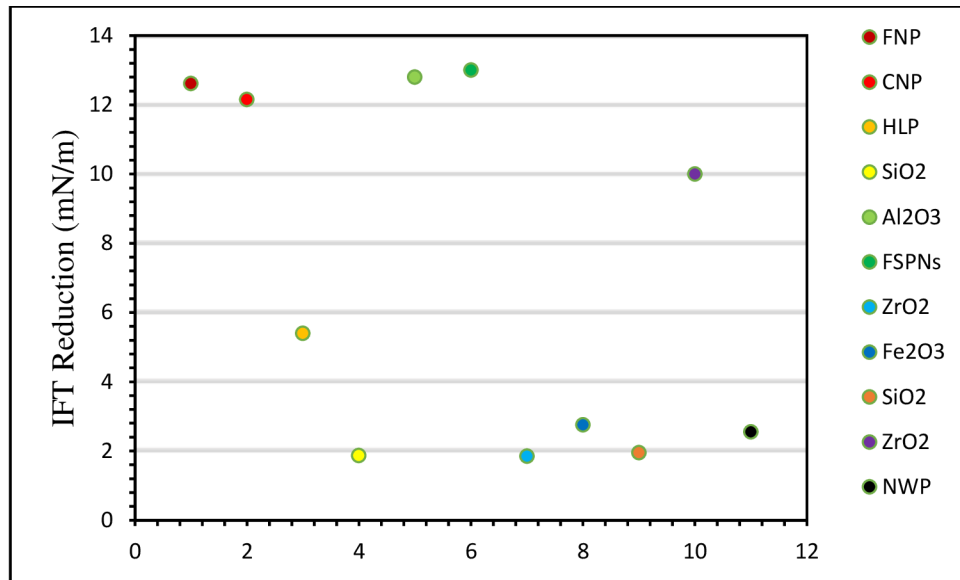


Figure 8 plotted graph of experimental data of reduction percentage of the interfacial tension using different NPs.

In addition, the attained values of IFT alone and IFT with NPs of each experiment are stated. Moreover, figure (8) illustrated the plotted graph of experimental data of the reduction percentage of the interfacial tension using NPs. The data are stated in table (1) experimentally obtained by different researchers from 2013 to 2019.

The wettability of the interior of the reservoir may be water-wet, oil-wet, or an intermediate kind of wet system, depending on the distribution of fluids around the rock grains (Lau et al. 2017).

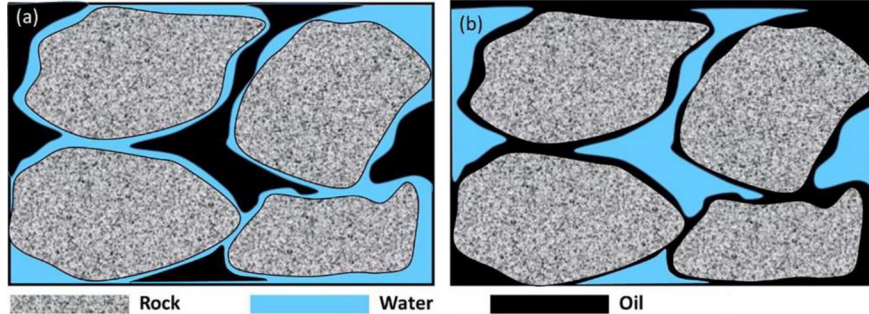


Figure 9 Fluid distributions in (a) water-wet and (b) oil-wet rock (Ali et al., 2018).

Table 3 stating the summarized data of conducted experiment by the following researchers: (Li and Torsæter, 2015), (Hendraningrat and Torsæter, 2014), (Nazari Moghaddam et al., 2015), (Azarshin, Moghadasi and A Aboosadi, 2017), (Mahbubul, 2019), (Esfandyari Bayat et al., 2014), (Roustaei et al., 2012), (Joonaki and Ghanaatian, 2014)

Table 3 A summary of previous works on effects of nanoparticles on contact angle.

NPs	NPs size (nm)	NPs Conc.	Porous media	Contact angle (°)		Ref.
				Clean	With NPs	
NSP	7	0.05–0.5 wt%	Sandstone cores	166	130	(Li and Torsæter, 2015)
CNP	18	0.05–0.5 wt%	Sandstone cores	166	124	(Li and Torsæter, 2015)
γ-Al₂O₃	10–20	0.5–1.5 wt%	Carbonate rocks	119.8	40	[38]
ZrO₂	24	0–0.1 g/cc	Carbonate cores	180	40	(Karimi et al., 2012)
Al₂O₃	4	100–1000 ppm	Sandstone cores	142	~0	(Giraldo et al., 2013)
SiO₂	40	0.05 wt%	Quartz plates	131.2	38.82	(Hendraningrat and Torsæter, 2014)
Al₂O₃	17	0.05 wt%	Quartz plates	131.2	28.6	(Hendraningrat and Torsæter, 2014)
ZrO₂	>35	0.05 g/100 ml	Carbonate cores	140.2	59.7	(Nazari Moghaddam et al., 2015)
MgO	>40	0.05 g/10 ml	Carbonate cores	140.2	98.2	(Nazari Moghaddam et al., 2015)
SiO₂	30–40	0.3 g/105 ml	Carbonate cores	140.2	68.5	(Nazari Moghaddam et al., 2015)
Al₂O₃	>40	0.03 g/100 ml	Carbonate cores	140.2	103.5	(Nazari Moghaddam et al., 2015)
SiO₂	12	1–4 g/L	Sandstone cores	135.5	66	(Nazari Moghaddam et al., 2015)

						2015)
SiO₂	10– 15	10gr/200 ml	Glass micromodel	134.4	54.52	(Azarshin, Moghadasi and A Aboosadi, 2017)
FSPNs*	10– 15	10gr/200 ml	Glass micromodel	134.4	23.71	(Azarshin, Moghadasi and A Aboosadi, 2017)
SiO₂	14	0.1–5 wt%	Glass micromodel	100	~0	(Maghzi et al., 2012)
Al₂O₃	20	0.05 wt%	Carbonate dolomite	70	52	(Mahbubul, 2019)
Al₂O₃	20	0.05 wt%	Carbonate dolomite	92	75	(Mahbubul, 2019)
Al₂O₃	20	0.05 wt%	Carbonate dolomite	85	62	(Mahbubul, 2019)
ZrO₂	40	0.05 wt%	Carbonate dolomite	70	60	(Mahbubul, 2019)
ZrO₂	40	0.05 wt%	Carbonate dolomite	92	84	(Mahbubul, 2019)
ZrO₂	40	0.05 wt%	Carbonate dolomite	85	71	(Mahbubul, 2019)
TiO₂	10– 30	50 mg/L	Limestone rocks	90	46	(Esfandyari Bayat et al., 2014)
HLP	10– 40	4 gr/L	Sandstone cores	135.5	95.44	(Hendraningrat and Torsæter, 2014)
NWP	10– 20	4 gr/L	Sandstone cores	135.5	81.88	(Roustaei et al., 2012)
Al₂O₃	~60	0.5–3 g/L	Sandstone cores	131	92	(Joonaki and Ghanaatian, 2014)
Fe₂O₃	40– 60	0.5–3 g/L	Sandstone cores	132.5	101	(Joonaki and Ghanaatian, 2014)
SiO₂	10– 30	0.5–3 g/L	Sandstone cores	134	82	(Joonaki and Ghanaatian, 2014)

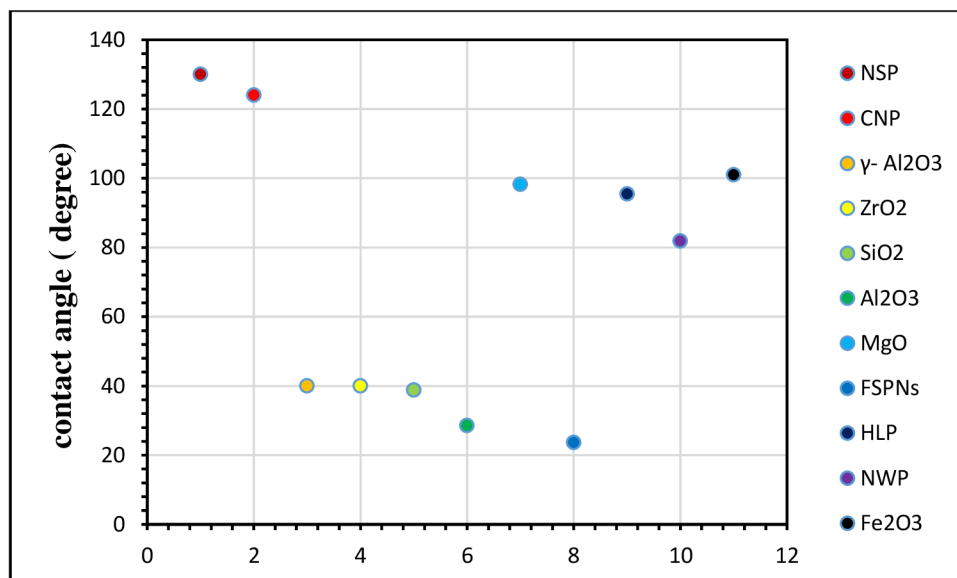


Figure 10 Plotted graph of obtained experimental data of different nanoparticles.

In addition, the attained values of contact angle alone and contact angle with NPs of each experiment are stated. Moreover, figure (10) illustrated the plotted graph of experimental data of the reduction percentage of the interfacial tension using NPs. The data are stated in table (2) experimentally obtained by different researchers from 2012 to 2019.

2.6. EOR in different reservoir conditions

The application of enhanced oil recovery methods (EOR), referred to as tertiary techniques, is predominantly observed in mature oil fields experiencing a decline in production following primary and secondary recovery techniques, or directly after the primary production stage. In order to draw out residual oil that is trapped in reservoir rock because of the existence of strong viscous and capillary forces as well as significant amount of IFT among the fluid and rock 'Enhanced Oil Recovery' methods involve the injection of gases or fluids. EOR methods are categorized based on the injected fluid type, production mechanism, and execution approach. These methods include thermal methods, chemical methods, miscible/immiscible gas injection methods. This paper examines the crucial factors that impact the effective execution of Enhanced Oil Recovery (EOR) projects. These factors include the various stages involved in EOR project implementation, the global crude oil price as a determining factor for initiating and justifying EOR processes, and the advancement of emerging technologies to enhance the efficiency of these processes (Maričić et al., 2014). NPs in suspension were analyzed to determine the surface charge, average hydrodynamic diameter, and solubility property in relation to salinity level and EDTA content. The chemical characteristics of both NPs in the modified high salt medium (HSM) altered similarly in relation to salinity level. Indeed, increased salinity resulted in increased ionic strength in the medium (Canuel et al., 2021). The zeta potential data showed that the ionic strength of HSM produced a negative surface charge on both NPs, with the charge intensity being greater for CuO-NPs than Fe₃O₄-NPs (Figure 11).

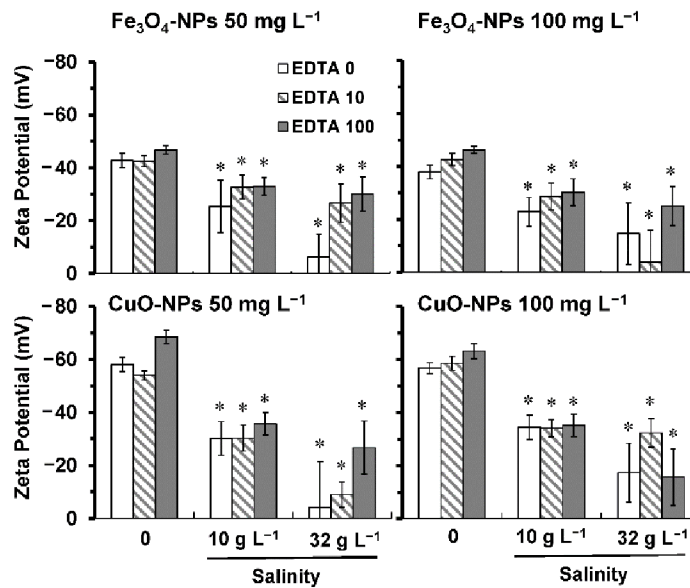


Figure 11 Zeta potential values of NPs in HSM (no salt added), and under two salinity conditions (10 and 32 g L⁻¹).

NPs were also exposed to EDTA concentrations: 0 mg L⁻¹ (white), 10 mg L⁻¹ (dash) and 100 mg L⁻¹ (gray). (*) For both NPs, the salinity significantly decreased ($p < 0.05$) the values of the zeta potential compared to the respective controls (no salt added), even in the presence of EDTA (determined by one-way ANOVA and Tukey post-hoc test) (Canuel et al., 2021). When both NPs were compared in freshwater HSM (Figure 14), CuO-NPs formed smaller agglomerates (100-250 nm) than Fe₃O₄-NPs (200–450 nm). In reality, due to electrostatic repulsion forces, a higher intensity of the surface charge caused the NPs dispersion to be more stable. Because the HSM had a neutral pH, the isoelectric point of Fe₃O₄-NPs was significantly lower and closer to neutral than that of CuO-NPs, explaining the lower intensity of the surface charge for Fe₃O₄-NPs. As a result, these zeta potential values explained the differential in agglomeration formation between the two NPs.

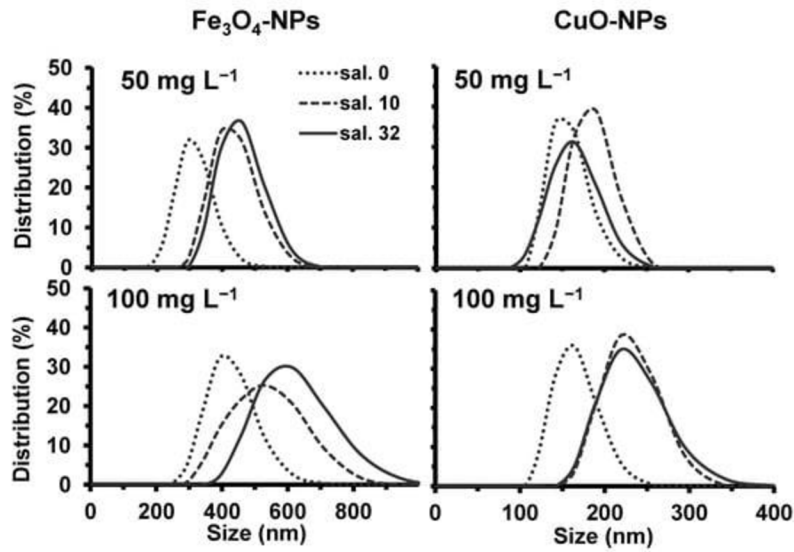


Figure 12 Hydrodynamic diameter distribution of Fe₃O₄ and CuO particle size in HSM (dots), and under two salinity conditions, 10 g L⁻¹ (dash) and 32 g L⁻¹ (line) (Canuel et al., 2021).

The influence of standing time (sedimentation time) on the effective thermal conductivity of nanofluids at varied Cu nanoparticle concentrations and temperatures is shown in Fig.14. Within 36 hours, there was no fluctuation in nanofluid effective thermal conductivity at 331.76 and 422.54 K. The absence of observable nanoparticle sedimentation in the test fluids indicates the nanofluid's stability.

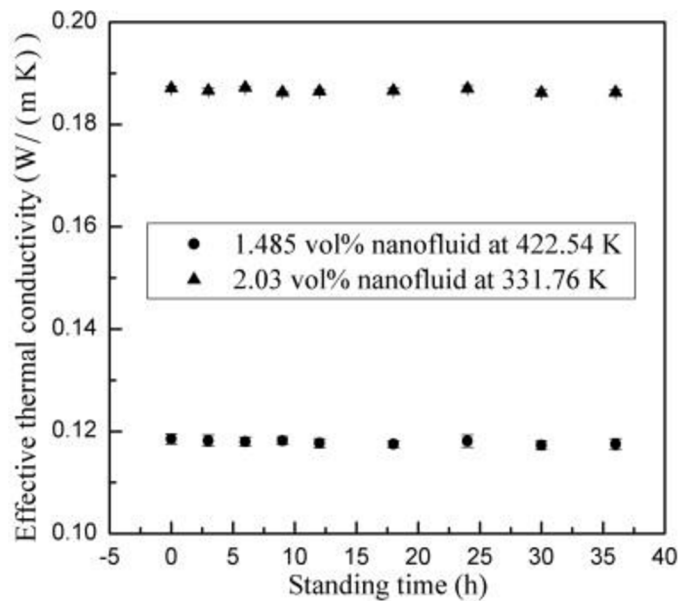


Figure 13 Effective thermal conductivities of nanofluids against standing time at different temperatures.

3.1 Materials

In order to carry out this laboratory experiment, we needed access to certain chemicals of a very high purity. These chemicals included methanol, ethanol, and toluene, and they were all supplied to us by the scientific research center at Soran university. In order to carry out our experiment, we need water in the form of distilled water as well as brine, both of which could be found at the labs at Soran University. In furthermore of this, the density of the crude oil that was delivered to us was 0.879 grams per cubic centimeter at 29.5 degrees API. Table 4 presents the chemical make-up of brine and crude oil for your perusal. As can be seen in figure 14, the carbonate rock samples that were utilized in the measurements of the contact angle were collected from outcrops of the Upper Qamchoqa formation surrounding Soran City.

Component	CO ₂	H ₂ S	C ₁	C ₂	C ₃	iC ₄	nC ₄	iC ₅	nC ₅	C ₆	C ₇	C ₇ ⁺
Molar Percent	0.0294	0.093	0.0285	0.40	2.4	.086	3.268	2.094	2.7529	5.66	9.32	82.31
				36	806	41		8		58		93
Specific gravity @ 60 °F =0.879												

Table 4 Composition of crude oil and brine

Component	Concentration in (ppm)
	Sea Water
Cl ⁻	11500
SO ₄ ²⁻	6860
HCO ₃ ⁻	180
Mg ²⁺	930
Ca ²⁺	1920
Na ⁺	7330
Fe ²⁺	Negligible
Sr ²⁺	Negligible
K ⁺	90
PH	7.67
TDS	33194



Figure 14 The rock sample and nano-composite that was used in this study.

3.2 Methodology

3.2.1 Preparation of nanofluid

Production of $\text{Fe}_2\text{O}_3/\text{Xanthan}$ NCs. These NCs were obtained from the scientific research center of Soran university and included various amounts of their respective created concentrations. The NCs were combined with brine and distilled water in varying concentrations of 250, 500, and 1000 ppm respectively. To produce these NCs, a Hot plate Stirrer was used to stir the mixture for six hours at a speed of 600 revolutions per minute (rpm), while the working temperature was maintained at less than 30 degrees Celsius. This was done to avoid the homogenizer from being overheated. Ultrasonic waves generated by an ultrasonic homogenizer were used to mix the NCs for a period of two hours in order to attain a high level of stability. As a consequence of this, the stability of the created NCs was visually observed and studied using clear containers throughout the course of time. In addition, the density, viscosity, conductivity, and pH of the NCs were measured by applying the instruments illustrated in figure 15, a density meter, a viscometer, a pH meter, and a conductivity meter, respectively.

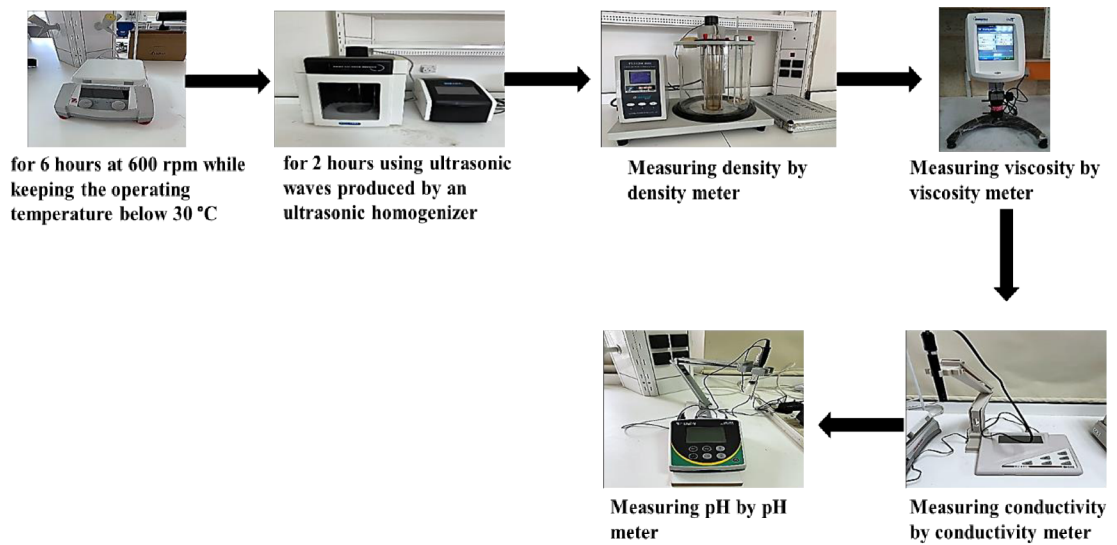


Figure 15 The devices are used to prepare NCs and measure their characteristics.

3.2.2 Preparation of rock thin sections

As shown in figure 16, a The experiment started out by forming core plug out of a piece of carbonate outcrop as the initial step. After creating the core plug by plugging machine the ends of the plug was not even therefore it was necessary to create an even end so that the slice would not give unprecise results therefore a core trimmer was used to create an even surface. After that in order to get rid of any impurities it was needed to put the plug into a Soxhlet extractor with toluene for 12 hours. After that the plug was taken out and put in the oven. A 24 hours stay in the oven in 60 Celsius degree was necessary to be able for the plug to be completely dry and to let the toluene evaporate and to get rid of any potential effect of toluene on it. Then the core plate is created in to 3.5 cm in dimeter Finally in order to make it oil wet a process called aging which is shown in figure 18 was made to the plates. It was soaked with oil and left in the oven for a week, a temperature of 70 Celsius degrees was used because it is needed to get to a reservoir condition. The plates are taken and it is washed by toluene so that no oil is left in the surface and we are left but only absorbed in the plate so that finally we get a plate that is is oil wet

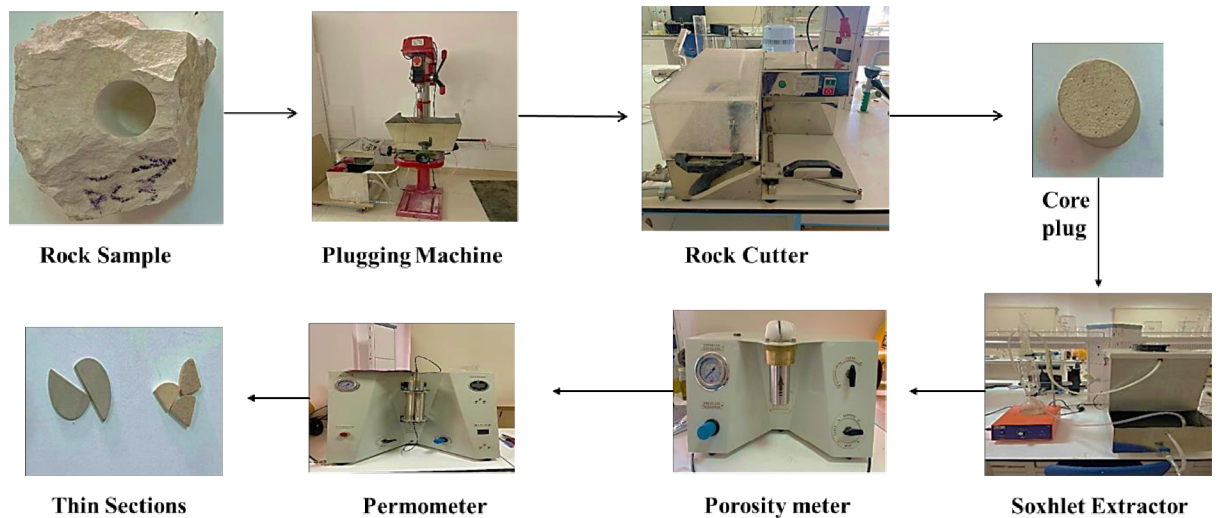


Figure 16 The procedure of preparing rock thin sections in this study

3.3.3 Interfacial tension measurement

One of the techniques to measure IFT is using a pendant drop technique. In this study, IFT was determined for the crude-oil/distilled-water and brine systems both with and without the addition of nanocomposite Fe₂O₃/Xanthan at concentrations of 250, 500, and 1000 ppm at three different temperatures (30 C°, 50 C°, and 70 C°) and at each temperature with three different pressures (500 ppm, 1000 ppm, and 1500 ppm) psi. Additionally, at each temperature, three different pressures were applied. The measurement by which it was done is shown in figure 17.

3.3.4. contact angle measurement

Because of its simplicity, sessile-drop technique is frequently regarded as the most extensively used method for surface-wetting characterization. The contact angle is calculated by examining the form of the droplet. Figure 18 IFT and contact angle measurements used in this study. The contact angle (CA) of crude oil on the surface of carbonate rocks with separate aqueous phases was determined using this approach. The

sessile drop method is dropping a drop of water or oil on a flat mineral surface and measuring the contact angle.

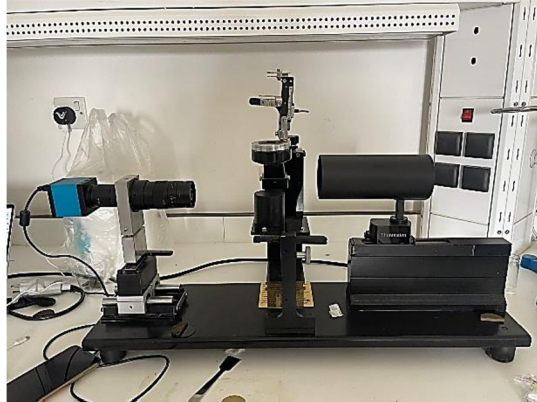


Figure 17 The IFT and contact angle measurements used in this study

In the end, a calculation was made to determine the contact angle, or CA, of crude oil droplets resting on the surface of each aged slice. In this study, the contact angle was measured at concentrations of 250, 500, and 1000 ppm in crude oil/distilled water and brine systems with and without the addition of nanocomposite Fe₂O₃/Xanthan at three different temperatures (30 C°, 50 C°, and 70 C°) and at each temperature with three different pressures (500, 1000, and 1500) psi. In addition, the test was performed at three different pressures (500, 1000, and 1500) psi.

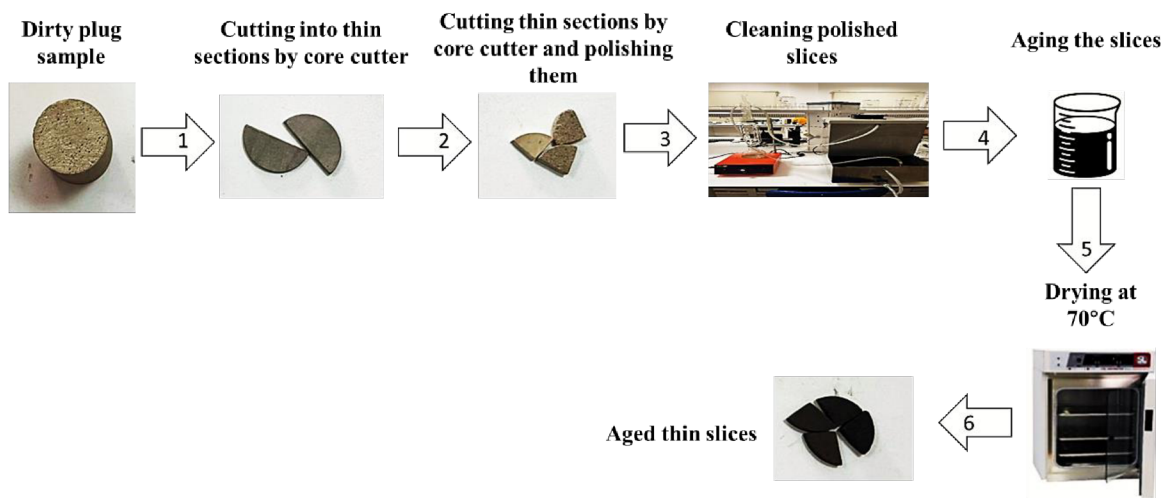


Figure 18 Ageing procedure of thin sections.

Chapter 4: Results and discussion

4.1 Characterization of nanofluid

The dispersion stability of the created NCs inside the dispersion media is crucial for determining the role of NPs exactly. In this section, the dispersion stability of colloidal solid particles inside the created NCs is tested and observed by measuring and monitoring pH, density, conductivity, and viscosity in three distinct NC concentrations (250,500,1000) ppm in DW and Brine as shown in figure 20. the conductivity at 250 ppm in DW was $141.2\mu\text{s}/\text{cm}$ and in SW was $60.6\text{ms}/\text{cm}$ as shown in figure 20a. in addition, with increasing concentration to 500 ppm the conductivity reduced in both DW and SW it was $32.6\mu\text{s}/\text{cm}$ in DW and $59.7\text{ms}/\text{cm}$ in SW. additionally, raising concentration to 1000 ppm the conductivity of both DW and SW rose it was $60.7\mu\text{s}/\text{cm}$ in DW and $60.1\text{ms}/\text{cm}$ in SW. The viscosity of both SW and DW increased as the concentration of NCs increased as shown in figure 20b. At 250ppm, the viscosity was 1.02 cp in DW and 1.26 cp in SW. With increasing concentration to 500 ppm, the viscosity of DW increased to 1.62 cp compared to 1.74 cp in SW, while it was 2.96 cp in DW and 2.88 in SW at 1000 ppm. The pH of DW rose with increasing NC content but not in SW as shown in figure 20c, first at 250 ppm it was 7.48 in DW and 6.82 in SW. After raising the concentration to 500 ppm, the pH of both DW and SW increased to 7.66 in DW and 7.34 in SW. However, when the concentration was increased to 1000 ppm, the pH in DW increased but declined in SW; it was 8.11 in DW and 7.13 in SW. Density increased with increasing NCs concentration in both SW and DW, but there was no significant difference as shown in figure 20d. At 250ppm, density was $0.9983\text{ gm}/\text{cm}^3$ in DW and $1.0284\text{ gm}/\text{cm}^3$ in SW; at 500ppm, density was $0.9986\text{ gm}/\text{cm}^3$ in DW and $1.0285\text{ gm}/\text{cm}^3$ in SW; and at 1000ppm, density was $0.9988\text{ gm}/\text{cm}^3$ in DW $1.0294\text{ gm}/\text{cm}^3$ with increasing concentration to 1000 ppm.

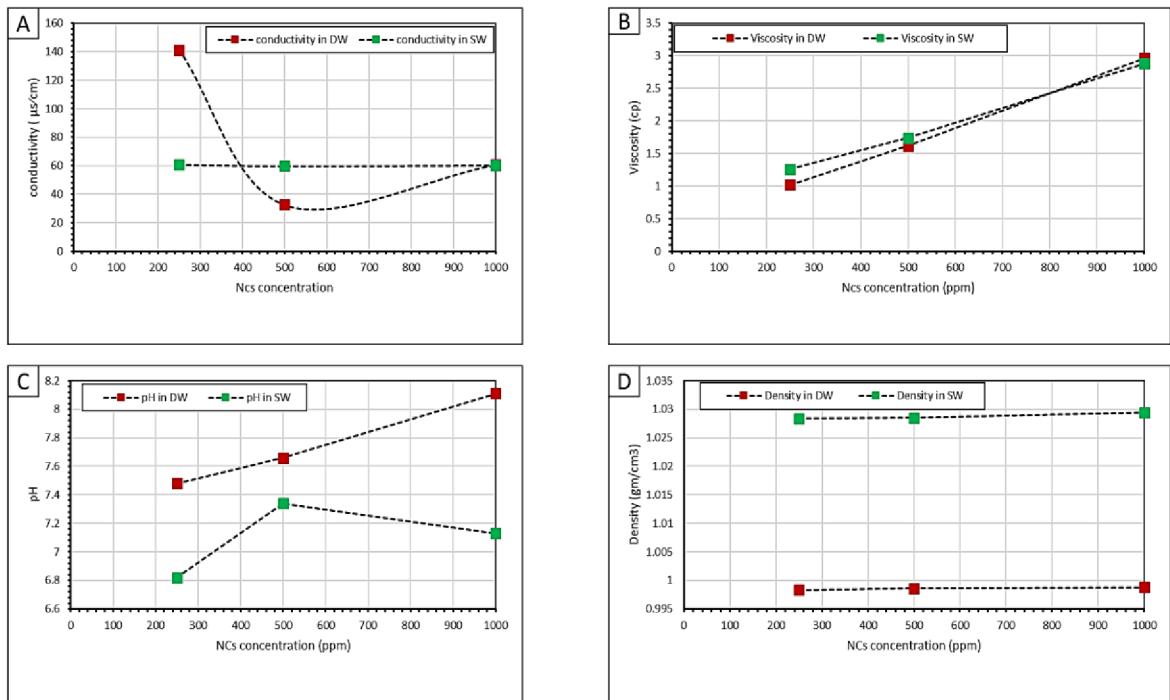


Figure 19 Impact of NCs concentration on a) conductivity b) viscosity c) pH and d) density.

4.2 Effect of NCs on wettability alteration

Contact angle was measured in DW and SW at three different concentrations of NCs (250 ppm, 500 ppm, and 1000 ppm) at three different temperatures (30 °C, 50 °C, and 70 °C), and at each temperature with three different pressures (500 psi, 1000 psi, and 1500 psi). As indicated in Table 5, the contact angle measured at 30, 50, and 70 degrees Celsius and 500 psi with a concentration of 250 ppm in SW and DW was 59.68 in 70 °C in SW and 47.34 in 30 °C in DW. When the concentration was increased to 500 ppm, the best result was 80.9 at 30 °C in SW and 81.42 at 50 °C in DW. When the concentration was increased to 1000 ppm, the best result was 51.96 at 30 °C in SW and 84.66 at 50 °C in DW.




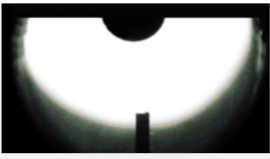
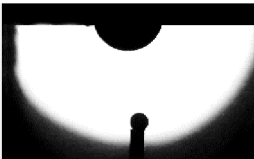
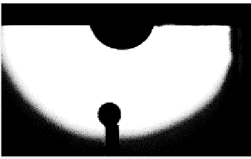












Table 5 Effect of temperature and nano concentration of contact angle in 500 psi.

water	Concentration (ppm)	30c,500 psi	50c, 500psi	70c,500psi
SW	250			
CA		81.89	60.48	59.68
SW	500			
CA		80.9	98.6	95.78
SW	1000			
CA		51.96	90.03	69.89
DW	250			
CA		47.34	81.42	78.57
DW	500			
CA		137.34	81.42	91.04
DW	1000			
CA		94.41	84.66	131.46

Furthermore, contact angle was measured in 1000 psi and the best one in SW250 ppm was discovered in 50 C° it was (49.62) and the worst one was in 70 C° it was (72.09) and in DW250 ppm the best one was in 30 C° it was (75.86) and the worst one was in 70 C° it was (78.57). With increasing concentration to 500 ppm, the best SW was in 50 c (53.51) and the worst was in 30 C° and 70 C° it had the same value (101.41) in DW500 ppm the best was in 70 C° (85.75) and the worst was in 30 C° (87.17). With concentrations rising to 1000 ppm,

the best SW was in 50 C° (88.58) and the worst was in 70 C° (88.81). In DW1000 ppm, the best was in 30 C° (74.34) and the worst was in 50 C° (113.47).

Table 6 Effect of temperature and nano concentration of contact angle in 1000 psi.

water	Concentration (ppm)	30c,1000 psi	50c, 1000psi	70c,1000psi
SW	250			
CA		63.62	49.62	72.09
SW	500			
CA		101.41	53.41	101.41
SW	1000			
CA		88.61	88.58	88.81
DW	250			
CA		75.86	77.2	80
DW	500			
CA		87.17	85.87	85.75
DW	1000			
CA		74.34	113.47	82.74

Furthermore, contact angle was evaluated at 1500 psi, with the best SW250 ppm identified in 50 C° (56.3) and the worst in 70 C° (68.4), and the best DW250 ppm discovered in 70 C° (80) and the worst in 30 C° (81.4). When the concentration was increased to 500 ppm, the best SW was in 30 C° (80.2), and the worst was in 70 C° (90.03). In DW500 ppm, the best was in 30 C° and 50 C° (81.42), and the worst was in 70 C° (121.59), as seen in Table 7.

Table 7 Effect of temperature and concentration on contact angle in 1500 psi.

water	Concentration (ppm)	30,1500 psi	50c, 1500psi	70c,1500psi
SW	250			
CA		66.9	56.3	68.4
SW	500			
CA		80.2	90.02	90.03
SW	1000			
CA		70.8	101.4	102.8
DW	250			
CA		81.4	81.42	80
DW	500			
CA		81.42	81.42	121.59
DW	1000			
CA		80.00	120.24	84.22

In addition, the best SW was in 30 C° (70.8), and the worst was in 70 C° (102.8) as concentrations increased to 1000 ppm. The best DW1000 ppm was in 30 C° (80), and the worst was in 50 C° (120.24).

4.3 Effect of NCs on interfacial tension

IFT was measured in DW and SW at three different concentrations of NCs (250 ppm, 500 ppm, and 1000 ppm) at three different temperatures (30 C°, 50 C°, and 70 C°), and at each temperature with three different pressures (500 psi, 1000 psi, and 1500 psi). First, IFT was measured at 250 ppm, 30 degrees Celsius, and 500 psi, and it was 11.892 mN/m in DW and 21.424 mN/m in SW. When the concentration was increased to 500 ppm, the IFT decreased to 2.645 mN/m in DW and 19.855 in SW. IFT increased to 6.653 mN/m in DW and declined to 16.594 mN/m in SW after raising concentration to 1000 ppm in the same circumstances as shown in figure 21. IFT rose to 14.671 mN/m in DW and 22.239 mN/m in SW as pressure was increased to 1000 psi at 30 degrees Celsius and 250 ppm. As shown in figure 21, after raising the concentration to 500 ppm compared to 500 psi, IFT reduced to 1.141 mN/m in DW and increased to 20.165 mN/m in SW. After raising the concentration to 1000 ppm, IFT decreased to 3.516 mN/m in DW and climbed to 19.799 mN/m in SW. After that, IFT measured at 30 degrees Celsius and 1500 ppm was 15.308 mN/m in DW and 20.166 mN/m in SW. After raising the concentration to 1000 ppm, the DW value reduced to 3.493 mN/m while the SW value climbed to 20.653 mN/m. Nonetheless, when the concentration was raised to 1000 ppm, the IFT climbed swiftly to 13.440 mN/m in DW and then fell to 17.682 mN/m, as shown in figure 21 in SW.

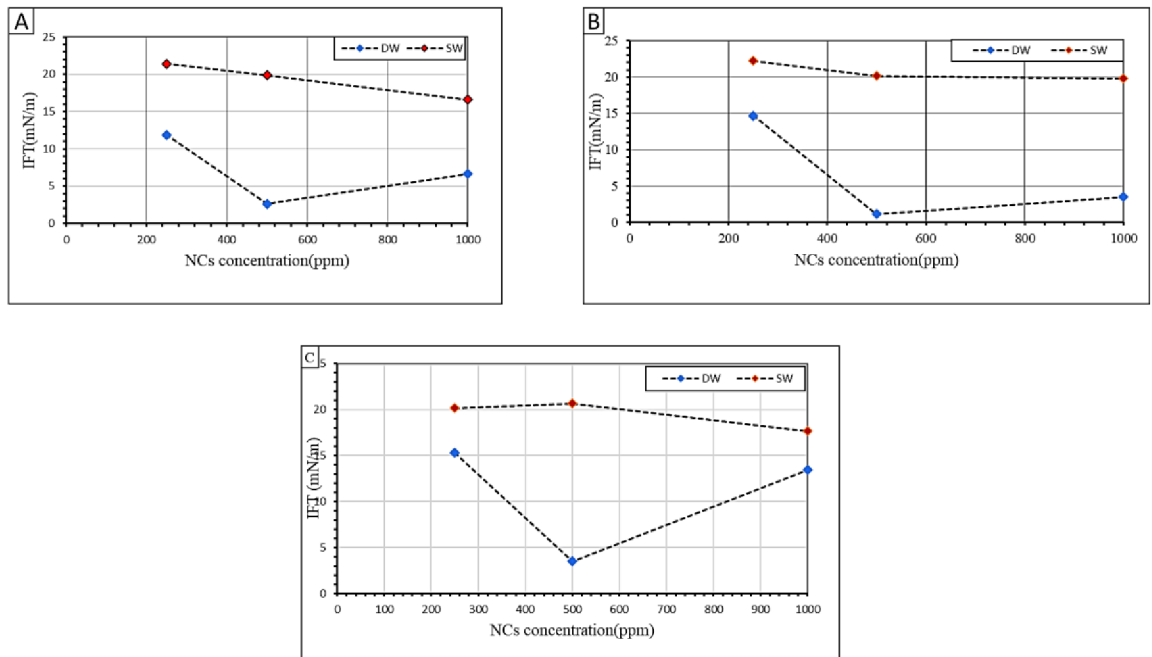


Figure 20 IFT values in DW and SW in three different concentrations (250ppm,500ppm,1000ppm) and pressures with constant temperature A) 30c, 500 psi. B) 30c, 1000psi. c) 30c, 1500 psi.

IFT measured at 50 degrees Celsius and 500 psi with a concentration of 250 ppm was 16.293 mN-m in DW and 19.655 mN/m in SW with the concentration rising to 500 ppm under the same conditions. IFT fell to 14.297 mN/m in DW and 19.271 mN/m in SW. When the concentration is increased to 1000ppm, the IFT decreases to 8.391 mN/m in DW and 15.353 mN/m in SW. IFT measured at 50 degrees Celsius and 1000 psi with a concentration of 250 ppm was 15.967 mN-m in DW and 19.279 mN/m in SW with a concentration of 500 ppm in the same conditions. IFT fell to 6.977 mN/m in DW and 19.435 mN/m in SW. After raising the concentration to 1000ppm, the IFT drops to 5.981 mN/m in DW and 17.020 mN/m in SW.

IFT was 9.377 mN-m in DW and 18.079 mN/m in SW when measured at 50 degrees Celsius and 1500 psi with a concentration of 250 ppm under the same conditions. In DW, IFT declined to 5.825 mN/m while increasing to 18.490 mN/m in SW. Subsequently, increasing the concentration to 1000 parts per million (ppm) results in a reduction of the interfacial tension (IFT) to 5.247 millinewtons per meter (mN/m) in distilled water (DW) and 17.839 mN/m in saltwater (SW), as depicted in Figure 22

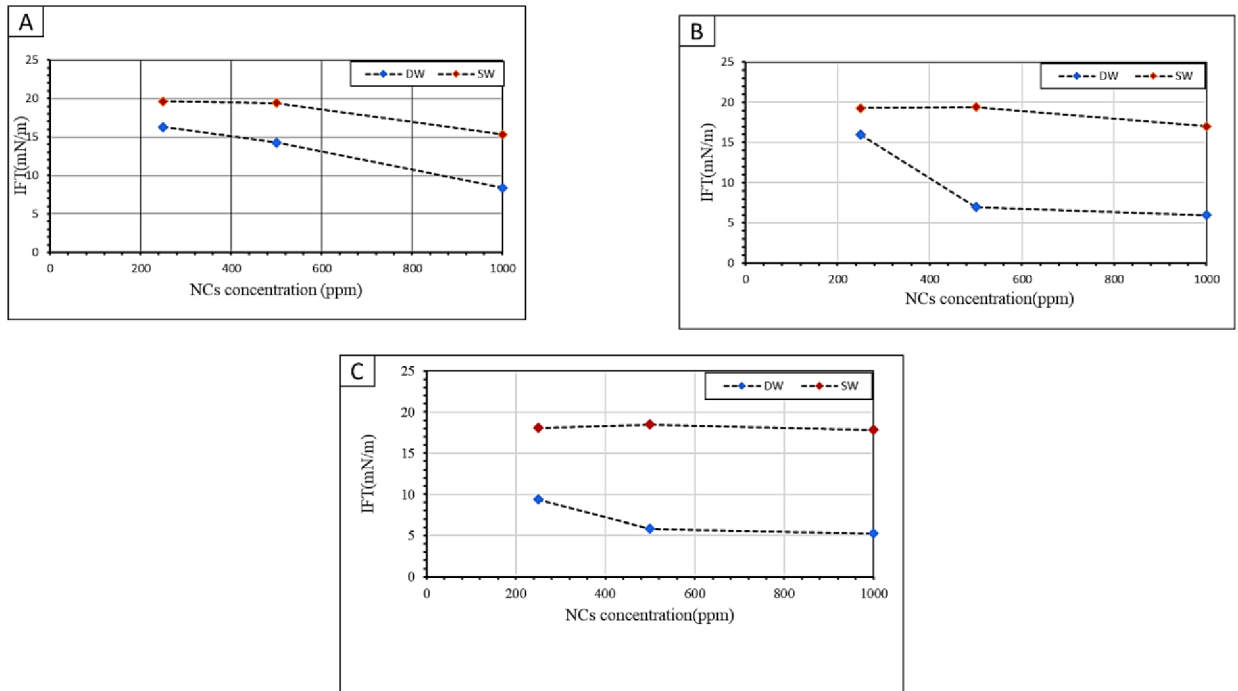


Figure 21 IFT values in DW and SW in three different concentrations (250ppm,500ppm,1000ppm) and pressures with constant temperature A) 50c, 500 psi. B) 50c, 1000psi. c) 50c, 1500 psi.

The interfacial tension (IFT) was measured to be 7.205 mN/m in distilled water (DW) and 18.248 mN/m in (SW) at a temperature of 70 degrees Celsius and a pressure of 500 psi. These measurements were obtained under the exact same circumstances, with a concentration of 250 ppm. In distilled water (DW), the interfacial tension (IFT) increased to 10.784 mN/m, while in (SW), it decreased to 17.044 mN/m. when we increased the concentration to 1000 parts per million (ppm), the interfacial tension (IFT) exhibited an improvement by , reaching 13.246 millinewtons per meter (mN/m) in distilled water (DW). Conversely, in saltwater (SW), the IFT saw a worsening to 15.003 mN/m. This data can be seen in Figure 26. an IFT value of 11.666 mN/m was found in distilled water (DW) at a temperature of 70 celsius degrees in a pressure of 1000 psi. after that a measurement was conducted under the the exact same temperature and pressure however with an increased concentration to 500 ppm was used resulting in an IFT value of 19.068 mN/m in SW. In distilled water (DW), the interfacial tension (IFT) decreased to 7.957 millinewtons per meter (mN/m), whereas in saltwater (SW), it decreased to 18.993 mN/m. As the concentration raised more to 1000 parts per million (ppm), the interfacial tension (IFT) exhibited an improvement by reaching a value of 10.874 millinewtons per meter (mN/m) in distilled

water (DW). Conversely, the IFT worsen to 16.326 mN/m in saltwater (SW), which can be seen in Figure 23. at a temperature of 70 degrees Celsius and a pressure of 1500 psi In deionized water (DW), the value of the IFT was found to be 9.502 mN/m at a concentration of 250 ppm. In seawater (SW), under the same circumstances, the IFT was measured to be 17.182 mN/m at a concentration of 500 ppm. In distilled water (DW), the interfacial tension (IFT) decreased to 8.412 millinewtons per meter (mN/m), whereas in saltwater (SW), it decreased to 15.013 mN/m. After increasing the concentration to 1000 parts per million (ppm), the interfacial tension (IFT) increased to 15.877 millinewtons per meter (mN/m) in distilled water (DW) and 17.562 mN/m in saltwater (SW), as depicted in Figure 23.

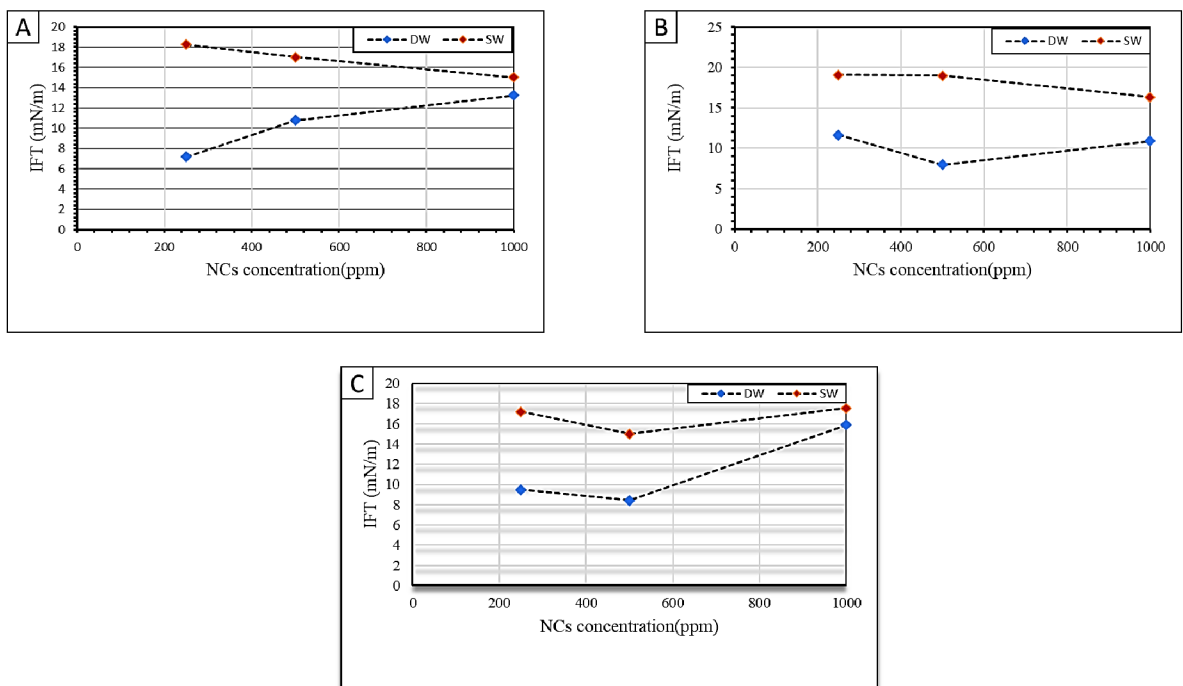


Figure 22 IFT values in DW and SW in three different concentrations (250ppm,500ppm,1000ppm) and pressures with constant temperature A) 70c, 500 psi. B) 70c, 1000psi. c) 70c, 1500psi.

Chapter 5: Conclusions and recommendations

5.1 conclusion

The influence of newly created nanocomposite known as Fe₂O₃/Xanthan nanocomposites on IFT reduction and wettability change during tertiary recovery operations was examined in this work under various experimental circumstances. Contact angle and IFT were measured in DW and SW at three different NC concentrations (250 ppm, 500 ppm, and 1000 ppm), three different temperatures (30 C°, 50 C°, and 70 C°), and three different pressures (500 psi, 1000 psi, and 1500 psi) in this study. As a consequence, the best IFT was measured in DW500 ppm at 30 C° and 1000 psi which had an IFT 1.141 mN/m. The finest contact angle in SW was SW250 ppm at 50 C° at 1000 psi lowered the contact angle to 49.62 degrees, whereas the finest on DW was DW250 ppm at 30 C° at 500 psi reduced the contact angle to 47.34 degrees.

5.2 Further recommendation

For further research subjects are the following:

- The effect of nanocomposite on recovery factor
- Using of green nano particles and comparing the results
- How does nano effect sweeping efficiency and how does it result in water consumption

References

- Abdallah, W., Buckley, J.S., Carnegie, A., Edwards, J., Herold, B., Fordham, E.J., Graue, A., Habashy, T.M., Seleznev, N., Signer, C. and Hussain, H., 2007. Fundamentals of wettability: Schlumberger Oilfield Review. Accessed November, 10, p.2020.
- Adeniyi, O.D., Nwalor, J.U. and Ako, C.T., 2008. Adeniyi OD, Nwalor JU and Ako CT (2008) A Review on Waterflooding Problems in Nigeria's Crude Oil Production, Journal of Dispersion Science & Technology (JDST), Taylor & Francis Group LLC, Philadelphia, USA, 29 (3): 362-365, 2008, ISSN: 0193-2691 print/1532-2351 online, [http://dx. doi. org/10.1080/01932690701716101](http://dx.doi.org/10.1080/01932690701716101).
- Ahmadi, M.A. and Shadizadeh, S.R., 2017. Nano-surfactant flooding in carbonate reservoirs: A mechanistic study. The European Physical Journal Plus, 132, pp.1-13.
- Ahmadi, Y., Mohammadi, M. and Sedighi, M., 2022. Introduction to chemical enhanced oil recovery. In Chemical Methods (pp. 1-32). Gulf Professional Publishing.
- Ahmed, T., 2010. Relative permeability concepts. Reserv. Eng. Handb, pp.288-330.
- Ahmed, T., 2019. Principles of waterflooding. Reservoir engineering handbook, pp.901-1107.
- Ali, J.A., Kolo, K., Manshad, A.K. and Mohammadi, A.H., 2018. Recent advances in application of nanotechnology in chemical enhanced oil recovery: Effects of nanoparticles on wettability alteration, interfacial tension reduction, and flooding. Egyptian journal of petroleum, 27(4), pp.1371-1383.
- Ali, J.A., Kolo, K., Manshad, A.K. and Stephen, K.D., 2021. Emerging applications of TiO₂/SiO₂/poly (acrylamide) nanocomposites within the engineered water EOR in carbonate reservoirs. Journal of Molecular Liquids, 322, p.114943.
- Al Ali, M. and Platko, P. eds., 2016. Advances and Trends in Engineering Sciences and Technologies II: Proceedings of the 2nd International Conference on Engineering Sciences and Technologies, 29 June-1 July 2016, High Tatras Mountains, Tatranské Matliare, Slovak Republic.
- Azarshin, S., Moghadasi, J. and A Aboosadi, Z., 2017. Surface functionalization of silica nanoparticles to improve the performance of water flooding in oil wet reservoirs. Energy Exploration & Exploitation, 35(6), pp.685-697.

Barzgar, E., 2021. Fractal properties of various clay minerals obtained from SEM images. *Geofluids*, 2021, pp.1-18

Barman, B.N., Cebolla, V.L., Mehrotra, A.K. and Mansfield, C.T., 2001. Petroleum and coal. *Analytical chemistry*, 73(12), pp.2791-2804.

Bhanvase, B.A., Barai, D.P., Sonawane, S.H., Kumar, N. and Sonawane, S.S., 2018. Intensified heat transfer rate with the use of nanofluids. In *Handbook of nanomaterials for industrial applications* (pp. 739-750). Elsevier.

Canuel, E., Vaz, C., Matias, W.G. and Dewez, D., 2021. Interaction Effect of EDTA, Salinity, and Oxide Nanoparticles on Alga *Chlamydomonas reinhardtii* and *Chlamydomonas euryale*. *Plants*, 10(10), p.2118.

Colombo, E.F., Shougarian, N., Sinha, K., Cascini, G. and de Weck, O.L., 2020. Value analysis for customizable modular product platforms: theory and case study. *Research in Engineering Design*, 31, pp.123-140.

El Shafey, A.M., 2017. Effect of nanoparticles and polymer nanoparticles implementation on chemical flooding, wettability and interfacial tension for the enhanced oil recovery processes. *African Journal of Engineering Research*, 5(3), pp.35-53.

Elsharafi, M.O., 2019, November. Preformed Particle Gels (PPGs) Compressibility Measurements in the Reservoirs Channels. In *ASME International Mechanical Engineering Congress and Exposition* (Vol. 59438, p. V006T06A053). American Society of Mechanical Engineers.

Emadi, S., Shadizadeh, S.R., Manshad, A.K., Rahimi, A.M. and Mohammadi, A.H., 2017. Effect of nano silica particles on Interfacial Tension (IFT) and mobility control of natural surfactant (Cedr Extraction) solution in enhanced oil recovery process by nano-surfactant flooding. *Journal of Molecular Liquids*, 248, pp.163-167.

Esfandyari Bayat, A., Junin, R., Samsuri, A., Piroozian, A. and Hokmabadi, M., 2014. Impact of metal oxide nanoparticles on enhanced oil recovery from limestone media at several temperatures. *Energy & fuels*, 28(10), pp.6255-6266.

- Esmaeilzadeh, P., Hosseinpour, N., Bahramian, A., Fakhroueian, Z. and Arya, S., 2014. Effect of ZrO₂ nanoparticles on the interfacial behavior of surfactant solutions at air–water and n-heptane–water interfaces. *Fluid Phase Equilibria*, 361, pp.289-295.
- Fanchi, J.R., 2010. Rock–fluid interactions. *Integrated Reservoir Asset Management*.
- Fernandes, B.R.B., 2014. Implicit and semi-implicit techniques for the compositional petroleum reservoir simulation based on volume balance.
- Gbadamosi, A.O., Junin, R., Manan, M.A., Agi, A. and Yusuff, A.S., 2019. An overview of chemical enhanced oil recovery: recent advances and prospects. *International Nano Letters*, 9, pp.171-202.
- Gbadamosi, A.O., Junin, R., Manan, M.A., Agi, A. and Yusuff, A.S., 2019. An overview of chemical enhanced oil recovery: recent advances and prospects. *International Nano Letters*, 9, pp.171-202.
- Gill, W.J. and Simon, J.L. (1998). *The Ultimate Resource 2*. *The Geographical Journal*, 164(2), p.220
- Giraldo, J., Benjumea, P., Lopera, S., Cortés, F.B. and Ruiz, M.A., 2013. Wettability alteration of sandstone cores by alumina-based nanofluids. *Energy & Fuels*, 27(7), pp.3659-3665.
- Golsanami, N., Fernando, S.G., Jayasuriya, M.N., Yan, W., Dong, H., Cui, L., Dong, X. and
- Guo, B., Sun, K. and Ghalambor, A., 2014. *Well productivity handbook*. Elsevier.
- Hendraningrat, L. and Torsæter, O., 2015. Metal oxide-based nanoparticles: revealing their potential to enhance oil recovery in different wettability systems. *Applied Nanoscience*, 5, pp.181-199.
- Hendraningrat, L., Li, S. and Torsaeter, O., 2013, July. Enhancing oil recovery of low-permeability Berea sandstone through optimized nanofluids concentration. In *SPE enhanced oil recovery conference*. OnePetro.

Höök, M., 2010. Coal and oil: The dark monarchs of global energy: Understanding supply and extraction patterns and their importance for future production (Doctoral dissertation, Acta Acta Universitatis Upsaliensis).

Joonaki, E. and Ghanaatian, S.J.P.S., 2014. The application of nanofluids for enhanced oil recovery: effects on interfacial tension and coreflooding process. *Petroleum Science and Technology*, 32(21), pp.2599-2607.

Karimi, A., Fakhroueian, Z., Bahramian, A., Pour Khiabani, N., Darabad, J.B., Azin, R. and Arya, S., 2012. Wettability alteration in carbonates using zirconium oxide nanofluids: EOR implications. *Energy & Fuels*, 26(2), pp.1028-1036.

Kaldi, V., 1992. Geological Applications of Capillary Pressure. A Review, *AAPG Bulletin*, 76, pp.840-850.

Karović-Maričić, V., Leković, B. and Danilović, D., 2014. Factors influencing successful implementation of enhanced oil recovery projects. *Podzemni radovi*, 22(25), pp.41-50.

Khalil, M., Jan, B.M., Tong, C.W. and Berawi, M.A., 2017. Advanced nanomaterials in oil and gas industry: Design, application and challenges. *Applied energy*, 191, pp.287-310.

Lau, H.C., Yu, M. and Nguyen, Q.P., 2017. Nanotechnology for oilfield applications: Challenges and impact. *Journal of Petroleum Science and Engineering*, 157, pp.1160-1169

Li, S. and Torsæter, O., 2015, January. The impact of nanoparticles adsorption and transport on wettability alteration of intermediate wet berea sandstone. In *SPE Middle East Unconventional Resources Conference and Exhibition*. OnePetro.

Li, S., Hendraningrat, L. and Torsaeter, O., 2013, March. Improved oil recovery by hydrophilic silica nanoparticles suspension: 2 phase flow experimental studies. In *IPTC 2013: International Petroleum Technology Conference* (pp. cp-350). EAGE Publications BV.

Li, Y., Dai, C., Zhou, H., Wang, X., Lv, W., Wu, Y. and Zhao, M., 2017. A novel nanofluid based on fluorescent carbon nanoparticles for enhanced oil recovery. *Industrial & Engineering Chemistry Research*, 56(44), pp.12464-12470.

Mahbubul, I.M., 2018. Preparation, characterization, properties, and application of nanofluid. William Andrew.

- Maroufi, P., Ayatollahi, S., Rahmanifard, H., Jahanmiri, A. and Riazi, M., 2013. Experimental investigation of secondary and tertiary oil recovery from fractured porous media. *Journal of Petroleum Exploration and Production Technology*, 3, pp.179-188.
- Manrique, E., Thomas, C., Ravikiran, R., Izadi, M., Lantz, M., Romero, J. and Alvarado, V., 2010, April. EOR: current status and opportunities. In *SPE Improved Oil Recovery Conference?* (pp. SPE-130113). SPE.
- McPhee, C., Reed, J. and Zubizarreta, I. (2015). Capillary Pressure. *Developments in Petroleum Science*, pp.449–517.
- Mehrjoo, H., Riazi, M. and Norouzi-Apourvari, S., 2022. A comprehensive review on the use of eco-friendly surfactants in oil industry. *Chemical Methods*, pp.357-399.
- Nazarahari, M.J., Manshad, A.K., Ali, M., Ali, J.A., Shafiei, A., Sajadi, S.M., Moradi, S., Iglauer, S. and Keshavarz, A., 2021. Impact of a novel biosynthesized nanocomposite (SiO₂@ Montmorilant@ Xanthan) on wettability shift and interfacial tension: Applications for enhanced oil recovery. *Fuel*, 298, p.120773.
- Raffa, P. and Druetta, P., 2019. Chemical enhanced oil recovery: advances in polymer flooding and nanotechnology. Walter de Gruyter GmbH & Co KG.
- Rahimi, A., Jami, M., Divandari, H. and Safari, M., 2022. Alkaline flooding. In *Chemical Methods* (pp. 141-220). Gulf Professional Publishing.
- Risal, A., Shikhrakar, S., Mishra, S., Kunwar, D., Karki, E., Shrestha, B., Khadka, S. and Holen, A., 2020. Anxiety and depression during COVID-19 pandemic among medical students in Nepal
- Roustaei, A., Moghadasi, J., Iran, A., Bagherzadeh, H. and Shahrabadi, A., 2012, June. An experimental investigation of polysilicon nanoparticles' recovery efficiencies through changes in interfacial tension and wettability alteration. In *SPE international oilfield nanotechnology conference and exhibition*. OnePetro.
- Roustaei, A., Saffarzadeh, S. and Mohammadi, M., 2013. An evaluation of modified silica nanoparticles' efficiency in enhancing oil recovery of light and intermediate oil reservoirs. *Egyptian Journal of Petroleum*, 22(3), pp.427-433.

- Saigal, T., Dong, H., Matyjaszewski, K. and Tilton, R.D., 2010. Pickering emulsions stabilized by nanoparticles with thermally responsive grafted polymer brushes. *Langmuir*, 26(19), pp.15200-15209.
- Sheng, J.J., 2010. *Modern chemical enhanced oil recovery: theory and practice*. Gulf Professional Publishing.
- Sheng, J.J., 2015. Status of surfactant EOR technology. *Petroleum*, 1(2), pp.97-105.
- Sircar, A., Rayavarapu, K., Bist, N., Yadav, K. and Singh, S., 2022. Applications of nanoparticles in enhanced oil recovery. *Petroleum Research*, 7(1), pp.77-90.
- Sircar, A., Rayavarapu, K., Bist, N., Yadav, K. and Singh, S., 2022. Applications of nanoparticles in enhanced oil recovery. *Petroleum Research*, 7(1), pp.77-90.
- Shingala, J., Shah, V., Dudhat, K. and Shah, M., 2020. Evolution of nanomaterials in petroleum industries: application and the challenges. *Journal of Petroleum Exploration and Production Technology*, 10, pp.3993-4006.
- Zaid, H.M., Ahmad Latiff, N.R. and Yahya, N., 2014. The effect of zinc oxide and aluminum oxide nanoparticles on interfacial tension and viscosity of nanofluids for enhanced oil recovery. In *Advanced Materials Research* (Vol. 1024, pp. 56-59). Trans Tech Publications Ltd.
- Wei, C., Huang, R., Ding, M., Yang, J. and Xiong, L., 2022. Characterization of saturation and pressure distribution based on deep learning for a typical carbonate reservoir in the Middle East. *Journal of Petroleum Science and Engineering*, 213, p.110442.
- Zargartalebi, M., Barati, N. and Kharrat, R., 2014. Influences of hydrophilic and hydrophobic silica nanoparticles on anionic surfactant properties: Interfacial and adsorption behaviors. *Journal of Petroleum Science and Engineering*, 119, pp.36-43.
- Zargartalebi, M., Kharrat, R. and Barati, N., 2015. Enhancement of surfactant flooding performance by the use of silica nanoparticles. *Fuel*, 143, pp.21-27.
- Zhang, H., Dong, M. and Zhao, S., 2012. Experimental study of the interaction between NaOH, surfactant, and polymer in reducing court heavy oil/brine interfacial tension. *Energy & fuels*, 26(6), pp.3644-3650.

Zhong, Y., Kuru, E., Zhang, H., Kuang, J. and She, J., 2019. Effect of fracturing fluid/shale rock interaction on the rock physical and mechanical properties, the proppant embedment depth and the fracture conductivity. *Rock Mechanics and Rock Engineering*, 52, pp.1011-1022.

Zhu, H., Wei, T., Couper, M.J. and Dahle, A.K., 2013. Effect of extrusion profile on surface microstructure and appearance of aluminum extrusions with different Fe contents. *JOM*, 65, pp.618-624.